

# Modeling Nonequilibrium Flow and Transport Processes Using HYDRUS

Jirka Šimůnek\* and Martinus Th. van Genuchten

Accurate process-based modeling of nonequilibrium water flow and solute transport remains a major challenge in vadose zone hydrology. Our objective here was to describe a wide range of nonequilibrium flow and transport modeling approaches available within the latest version of the HYDRUS-1D software package. The formulations range from classical models simulating uniform flow and transport, to relatively traditional mobile-immobile water physical and two-site chemical nonequilibrium models, to more complex dual-permeability models that consider both physical and chemical nonequilibrium. The models are divided into three groups: (i) physical nonequilibrium transport models, (ii) chemical nonequilibrium transport models, and (iii) physical and chemical nonequilibrium transport models. Physical nonequilibrium models include the Mobile-Immobile Water Model, Dual-Porosity Model, Dual-Permeability Model, and Dual-Permeability Model with Immobile Water. Chemical nonequilibrium models include the One Kinetic Site Model, the Two-Site Model, and the Two Kinetic Sites Model. Finally, physical and chemical nonequilibrium transport models include the Dual-Porosity Model with One Kinetic Site and the Dual-Permeability Model with Two-Site Sorption. Example calculations using the different types of nonequilibrium models are presented. Implications for the formulation of the inverse problem are also discussed. The many different models that have been developed over the years for nonequilibrium flow and transport reflect the multitude of often simultaneous processes that can govern nonequilibrium and preferential flow at the field scale.

THERE IS increasing evidence that flow and transport processes in soils often cannot be described using classical models that assume uniform flow and transport (e.g., Nkedi-Kizza et al., 1984; Hendrickx and Flury, 2001; Pot et al., 2005; Köhne et al., 2006). Many laboratory and field experiments have demonstrated the presence of nonequilibrium flow and transport conditions in soils. Nonequilibrium water flow and solute transport in the unsaturated zone can be simulated at present by means of a large number of models of various degrees of complexity and dimensionality. Modeling approaches range from relatively simple analytical solutions for solute transport (e.g., van Genuchten, 1981; Toride et al., 1993) to complex numerical codes (e.g., Šimůnek et al., 2005; Jacques and Šimůnek, 2005). While such programs as STANMOD (Šimůnek et al., 1999) that implement analytical solutions undoubtedly will remain useful for simplified analyses of solute transport during steady-state flow (e.g., for

analyzing solute breakthrough curves measured in the laboratory, or for initial or approximate analysis of field-scale transport problems), numerical models are now increasingly being used since they can be applied more readily than analytical models to realistic laboratory and field problems. The use of numerical models has been further popularized during the last 20 yr or so because of the appearance of appropriate software packages in both the public and commercial domains and the development of increasingly sophisticated graphics-based interfaces that can simplify their use tremendously.

Attempts to describe nonequilibrium transport have traditionally been developed along two lines: physical and chemical nonequilibrium models (van Genuchten and Cleary, 1979). While physical nonequilibrium models assume that nonequilibrium flow or transport is caused by physical factors (e.g., van Genuchten and Wierenga, 1976), chemical nonequilibrium models assume that chemical factors are the cause of nonequilibrium transport (e.g., Selim et al., 1976; van Genuchten and Wagenet, 1989). Only a few researchers (e.g., Brusseau et al., 1989; Selim et al., 1999; Pot et al., 2005) have combined the physical and chemical nonequilibrium approaches to account for both possible causes of nonequilibrium, thus improving the description of solute transport in soils.

Over the years, several publicly available numerical codes have been developed that consider a number of options for simulating nonequilibrium water flow and solute transport (e.g., Pruess, 1991; Jarvis, 1994; van Dam et al., 1997). Unique to the HYDRUS-1D software package (Šimůnek et al., 2005, 2008) is the wide range of approaches that can be selected for

J. Šimůnek, Dep. of Environmental Sciences, Univ. of California, Riverside, CA 92521; M.Th. van Genuchten, USDA-ARS, U.S. Salinity Lab., 450 West Big Springs Rd., Riverside, CA 92507. Received 17 Apr. 2007. \*Corresponding author (Jiri.Simunek@ucr.edu).

Vadose Zone J. 7:782–797  
doi:10.2136/vzj2007.0074

© Soil Science Society of America  
677 S. Segoe Rd. Madison, WI 53711 USA.  
All rights reserved. No part of this periodical may be reproduced or transmitted in any form or by any means, electronic or mechanical, including photocopying, recording, or any information storage and retrieval system, without permission in writing from the publisher.

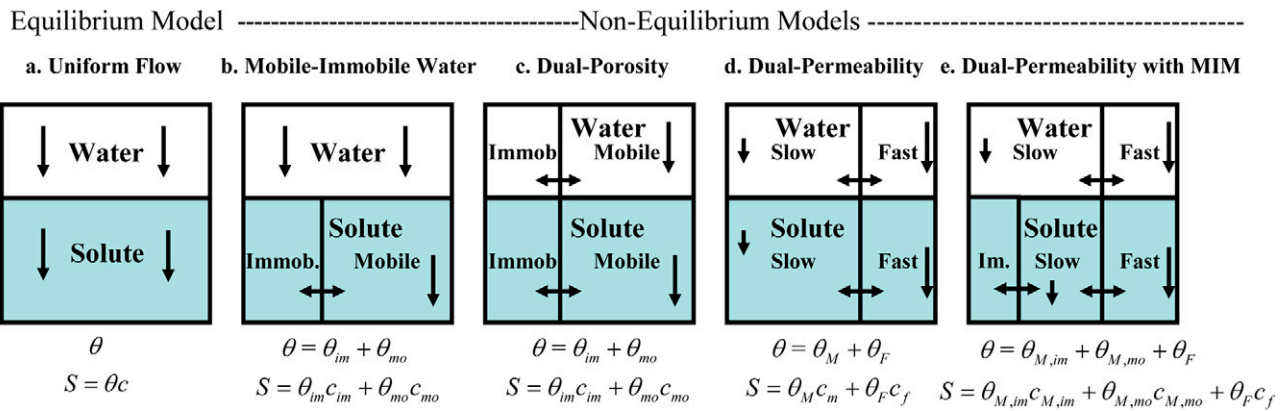


FIG. 1. Conceptual physical nonequilibrium models for water flow and solute transport. In the plots,  $\theta$  is the water content,  $\theta_{mo}$  and  $\theta_{im}$  in (b) and (c) are water contents of the mobile and immobile flow regions, respectively;  $\theta_M$  and  $\theta_F$  in (d) are water contents of the matrix and macropore (fracture) regions, respectively, and  $\theta_{M,mo}$ ,  $\theta_{M,im}$ , and  $\theta_F$  in (e) are water contents of the mobile and immobile flow regions of the matrix domain, and in the macropore (fracture) domain, respectively;  $c$  are concentrations of corresponding regions, with subscripts having the same meaning as for water contents, while  $S$  is the total solute content of the liquid phase.

simulating nonequilibrium processes. Our objective here is to describe the large number of physical and chemical nonequilibrium approaches available in the latest version of HYDRUS-1D (Šimůnek et al., 2008). The models range from classical models simulating uniform flow and transport, to traditional dual-porosity physical and two-site chemical nonequilibrium models, to complex dual-permeability models that consider both physical and chemical nonequilibrium. Since our focus is mainly on solute transport and since the nonequilibrium models for water flow have been reviewed relatively recently (Šimůnek et al., 2003), we only very briefly review here the governing water flow equations to define variables later used in the solute transport equations. We will present several examples calculated with the different nonequilibrium approaches to show the effect of various transport and reaction parameters, and to demonstrate the consequences of increased complexity in the models. Implications for the formulation of the inverse problem are also discussed.

### Overview of Conceptual Models

A large number of alternative physical and chemical nonequilibrium models can be formulated. Figures 1 and 2 show schematics of a range of possible physical equilibrium and nonequilibrium models for water flow and solute transport. Figure 3 shows similar schematics of various chemical nonequilibrium models that have been incorporated into HYDRUS-1D. Traditional flow and transport models are based on the classical description of uniform flow and transport in soils (the Uniform Flow Model in Fig. 1a and 2a). In this model, the porous medium is viewed as a collection of impermeable soil particles (or of impermeable soil aggregates or rock fragments), separated by pores or fractures through which flow and transport takes place. Variably saturated water flow through such a porous system is usually described using the Richards equation and solute transport using the classical advection–dispersion equation. Definitions

of various water contents and concentrations used in the different models are given in the Appendix.

A hierarchical set of physical nonequilibrium flow and transport models can be derived from the Uniform Flow Model. The equilibrium flow and transport model can be modified by assuming that the soil particles or aggregates have their own microporosity and that water present in these micropores is immobile (the Mobile–Immobile Water Model in Fig. 1b and 2b). While the water content in the micropore domain is constant in time, dissolved solutes can move into and out of this immobile domain by molecular diffusion (e.g., van Genuchten and Wierenga, 1976). This simple modification leads to physical nonequilibrium solute transport while still maintaining uniform water flow.

The mobile–immobile water model can be further expanded by assuming that both water and solute can move into and out of the immobile domain (Šimůnek et al., 2003), leading to the Dual-Porosity Model in Fig. 1c and 2c. While the water content inside of the soil particles or aggregates is assumed to be constant in the Mobile–Immobile Water Model, it can vary in the Dual-Porosity Model since the immobile domain is now allowed to dry out or rewet during drying and wetting processes. Water flow into and out of the immobile zone is usually described using a first-order rate process. Solute can move into the immobile domain of the Dual-Porosity Model by both molecular diffusion and advection with flowing (exchanging) water. Since water can

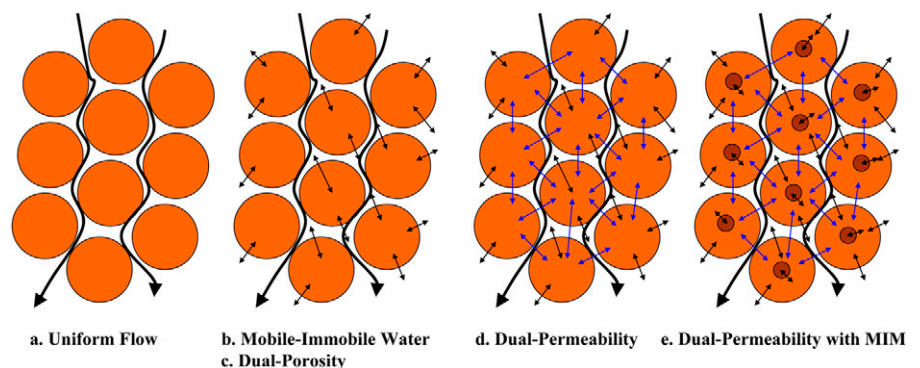


FIG. 2. Conceptual physical nonequilibrium models for water flow and solute transport.

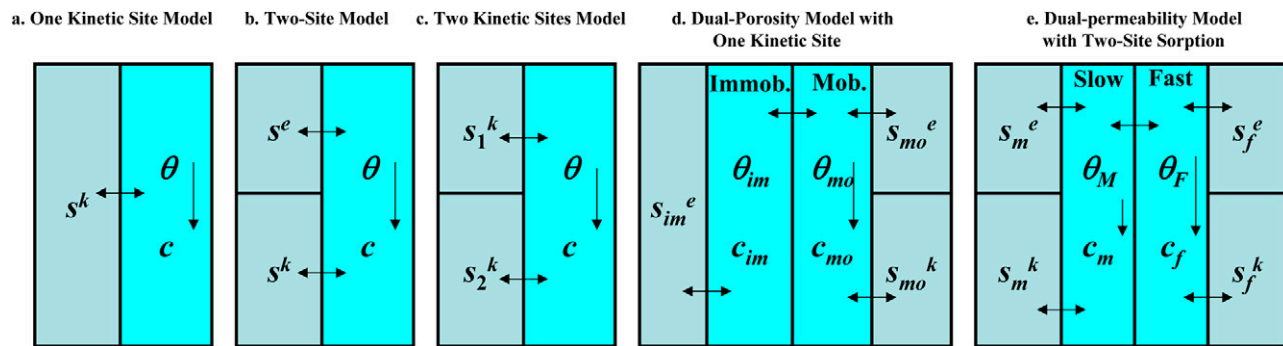


FIG. 3. Conceptual chemical nonequilibrium models for reactive solute transport. In the plots,  $\theta$  is the water content,  $\theta_{mo}$  and  $\theta_{im}$  in (d) are water contents of the mobile and immobile flow regions, respectively;  $\theta_M$  and  $\theta_F$  in (e) are water contents of the matrix and macropore (fracture) regions, respectively;  $c$  are concentrations of the corresponding regions,  $s^e$  are sorbed concentrations in equilibrium with the liquid concentrations of the corresponding regions, and  $s^k$  are kinetically sorbed solute concentrations of the corresponding regions.

move from the main pore system into the soil aggregates and vice versa, but not directly between the aggregates themselves, water in the aggregates can be considered immobile from a larger scale point of view.

The limitation of water not being allowed to move directly between aggregates is overcome in a Dual-Permeability Model (e.g., Gerke and van Genuchten, 1993a,b). Water and solutes in such models also move directly between soil aggregates, as shown in Fig. 1d and 2d. Dual-permeability models assume that the porous medium consists of two overlapping pore domains, with water flowing relatively fast in one domain (often called the macropore, fracture, or interporosity domain) when close to full saturation, and slow in the other domain (often referred to as the micropore, matrix, or intraporosity domain). Like the Dual-Porosity Model, the Dual-Permeability Model allows the transfer of both water and solutes between the two pore regions.

Finally, the Dual-Permeability Model can be further refined by assuming that inside of the matrix domain an additional immobile region exists into which solute can move by molecular diffusion (the Dual-Permeability Model with MIM in Fig. 1e and 2e).

Chemical nonequilibrium models implemented into HYDRUS-1D are schematically shown in Fig. 3. The simplest chemical nonequilibrium model assumes that sorption is a kinetic process (the One Kinetic Site Model in Fig. 3a), usually described by means of a first-order rate equation. This model can be expanded into a Two-Site Sorption model by assuming that the sorption sites can be divided into two fractions (e.g., Selim et al., 1976; van Genuchten and Wagenet, 1989). The simplest two-site sorption model arises when sorption on one fraction of the sorption sites is assumed to be instantaneous, while kinetic sorption occurs on the second fraction (Two-Site Model in Fig. 3b). This model can be further expanded by assuming that sorption on both fractions is kinetic and proceeds at different rates (the Two Kinetic Sites Model in Fig. 3c). The Two Kinetic Sites Model reduces to the Two-Site Model when one rate is so high that it can be considered instantaneous, to the One Kinetic Site Model when both rates are the same, or to the chemical equilibrium model when both rates are so high that they can be considered instantaneous.

The different models discussed thus far involve either physical or chemical nonequilibrium. Many transport situations will

involve both types of nonequilibrium. One obvious example occurs during transport through an aggregated laboratory soil column involving steady-state water flow (either fully saturated or unsaturated) when both a conservative tracer (no sorption) and a reactive solute are used. The collected tracer breakthrough curve may then display typical features reflecting nonequilibrium, such as a relatively rapid initial breakthrough followed by extensive tailing. Since the tracer is nonreactive, this nonequilibrium must be caused by physical factors. When the reactive solute is additionally sorbed kinetically to the solid phase (an indication of a chemical nonequilibrium), the use of a model is required that simultaneously considers both physical and chemical nonequilibrium.

The resulting combined physical and chemical nonequilibrium approach may be simulated with HYDRUS-1D using the Dual-Porosity Model with One Kinetic Site (Fig. 3d). This model considers water flow and solute transport in a dual-porosity system (or a medium with mobile-immobile water) while assuming that sorption in the immobile zone is instantaneous. Following the two-site kinetic sorption concept, however, the sorption sites in contact with the mobile zone are now divided into two fractions, subject to either instantaneous or kinetic sorption. Since the residence time of solutes in the immobile domain is relatively large, equilibrium probably exists between the solution and the sorption complex here, in which case there is no need to consider kinetic sorption in the immobile domain. The model, on the other hand, assumes the presence of kinetic sorption sites in contact with the mobile zone since water can move relatively fast in the macropore domain and thus prevent chemical equilibrium.

Finally, chemical nonequilibrium can also be combined with the Dual-Permeability Model. This last nonequilibrium option implemented into HYDRUS-1D (the Dual-Permeability Model with Two-Site Sorption in Fig. 3e) assumes that equilibrium and kinetic sites exist in both the macropore (fracture) and micropore (matrix) domains.

A complete list of the different models summarized here, and described in more detail below, is given in Table 1, including the specific equations used for the water flow and solute transport models. The table additionally lists the various parameters, and their total number, that will appear in any particular solute transport model when used for steady-state flow conditions.

TABLE 1. Equilibrium and nonequilibrium models in HYDRUS-1D, their governing equations, and the number of solute transport parameters for each model under steady-state water flow conditions.

Model name	Water flow equation(s)	Solute transport equation(s)	At steady-state water flow	
			No. of parameters	Parameters
Equilibrium model				
Uniform flow and transport	[1]	[6]	4	$\theta, q, \lambda, K_d$
Physical nonequilibrium models				
Mobile-immobile water model	[1]	[2], [11]	7	$\theta_{mo}, \theta_{im}, q_{mo}, \lambda_{mo}, K_d, f_{mo}, \omega_{mim}$
Dual-porosity model	[2], [3]	[11]	7	$\theta_{mo}, \theta_{im}, q_{mo}, \lambda_{mo}, K_d, f_{mo}, \omega_{mim}$
Dual-permeability model	[4], [5]	[12]	9	$\theta_m, \theta_f, q_m, q_f, \lambda_m, \lambda_f, K_{dm}, K_{df}, \omega_{dp}$
Dual-permeability model with immobile water	[4], [5]	[13], [14]	12	$\theta_{m,m'}, \theta_{im,m'}, \theta_f, q_m, q_f, \lambda_m, \lambda_f, K_{dm}, K_{df}, f_m, \omega_{dp}, \omega_{pdm}$
Chemical nonequilibrium models				
One kinetic site model	[1]	[6], [15]	5	$\theta, q, \lambda, K_d, \alpha_k$
Two-site model	[1]	[16], [17]	6	$\theta, q, \lambda, K_d, f_e, \alpha_k$
Two kinetic sites model	[1]	[18]	7	$\theta, q, \lambda, k_{a1}, k_{d1}, k_{a2}, k_{d2}$
Physical and chemical nonequilibrium models				
Dual-porosity model with one kinetic site	[2], [3]	[2], [20], [21]	9	$\theta_{mo}, \theta_{im}, q_{mo}, \lambda_{mo}, K_d, f_{mo}, f_{em}, \omega_{ph}, \alpha_{ch}$
Dual-permeability model with two-site sorption	[4], [5]	[22]	13	$\theta_m, \theta_f, q_m, q_f, \lambda_m, \lambda_f, K_{dm}, K_{df}, f_m, f_f, \omega_{dp}, \alpha_{ch,m}, \alpha_{ch,f}$

## Specific Models for Water Flow

We will briefly review the governing equations for both equilibrium (uniform) water flow and for nonequilibrium flow in dual-porosity and dual-permeability systems. Subsequently we will describe various solute transport models that consider either physical or chemical nonequilibrium and models that consider simultaneously both physical and chemical nonequilibrium.

### Uniform Flow Model

Numerical models for water flow in soils (Fig. 1a and 2a) are usually based on the following equation:

$$\frac{\partial \theta(h)}{\partial t} = \frac{\partial}{\partial z} \left[ K(h) \left( \frac{\partial h}{\partial z} + 1 \right) \right] - S \quad [1]$$

or its extensions (e.g., for two- and three-dimensional systems). In Eq. [1], often referred to as the Richards equation,  $z$  is the vertical coordinate positive upward [L],  $t$  is time [T],  $h$  is the pressure head [L],  $\theta$  is the water content [ $L^3 L^{-3}$ ],  $S$  is a sink term representing root water uptake or some other source or sink [ $T^{-1}$ ], and  $K(h)$  is the unsaturated hydraulic conductivity function, often given as the product of the relative hydraulic conductivity,  $K_r$  (dimensionless), and the saturated hydraulic conductivity,  $K_s$  [ $L T^{-1}$ ]. Solutions of the Richards Eq. [1] require knowledge of the unsaturated soil hydraulic functions made up of the soil water retention curve,  $\theta(h)$ , which describes the relationship between the water content  $\theta$  and the pressure head  $h$ , and the unsaturated hydraulic conductivity function,  $K(h)$ , which defines the hydraulic conductivity  $K$  as a function of  $h$  or  $\theta$ . HYDRUS-1D considers both relatively traditional models (Brooks and Corey, 1964; van Genuchten, 1980) for the hydraulic functions, as well as more recent alternative single- (e.g., Kosugi, 1996) and dual-porosity (Durner, 1994) models.

### Dual-Porosity Model

Dual-porosity models (Fig. 1c and 2c) assume that water flow is restricted to the macropores (or interaggregate pores and fractures), and that water in the matrix (intraaggregate pores or the rock matrix) does not move at all. This conceptualiza-

tion leads to two-region type flow and transport models (van Genuchten and Wierenga, 1976) that partition the liquid phase into mobile (flowing, interaggregate),  $\theta_{mo}$ , and immobile (stagnant, intraaggregate),  $\theta_{im}$ , regions [ $L^3 L^{-3}$ ]:

$$\theta = \theta_{mo} + \theta_{im} \quad [2]$$

The dual-porosity formulation for water flow can be based on a mixed formulation of the Richards Eq. [1] to describe water flow in the macropores (the preferential flow pathways) and a mass balance equation to describe moisture dynamics in the matrix as follows (Šimůnek et al., 2003):

$$\frac{\partial \theta_{mo}(h_{mo})}{\partial t} = \frac{\partial}{\partial z} \left[ K(h_{mo}) \left( \frac{\partial h_{mo}}{\partial z} + 1 \right) \right] - S_{mo}(h_{mo}) - \Gamma_w \quad [3]$$

$\frac{\partial \theta_{im}(h_{im})}{\partial t} = -S_{im}(h_{im}) + \Gamma_w$   
 where  $S_{mo}$  and  $S_{im}$  are sink terms for the mobile and immobile regions, respectively [ $T^{-1}$ ], and  $\Gamma_w$  is the transfer rate for water between the inter- and intraaggregate pore domains [ $T^{-1}$ ]. Šimůnek et al. (2003) and Köhne et al. (2004) discussed different formulations that can be used to evaluate the mass transfer rate  $\Gamma_w$ .

### Dual-Permeability Model

Different dual-permeability approaches (Fig. 1d, 1e, 2d, and 2e) may be used to describe flow and transport in structured media. While some models invoke similar equations for flow in the fracture and matrix regions, others use different formulations for the two regions. A typical example of the first approach, implemented in HYDRUS-1D, is the work of Gerke and van Genuchten (1993a,b, 1996), who applied the Richards equation to each of the two pore regions. The flow equations for the macropore (fracture) (subscript f) and matrix (subscript m) pore systems in their approach are given by

$$\frac{\partial \theta_f(h_f)}{\partial t} = \frac{\partial}{\partial z} \left[ K_f(h_f) \left( \frac{\partial h_f}{\partial z} + 1 \right) \right] - S_f(h_f) - \frac{\Gamma_w}{w}$$

$$\frac{\partial \theta_m(h_m)}{\partial t} = \frac{\partial}{\partial z} \left[ K_m(h_m) \left( \frac{\partial h_m}{\partial z} + 1 \right) \right] - S_m(h_m) + \frac{\Gamma_w}{1-w}$$
[4]

where  $w$  is the ratio of the volumes of the macropore or fracture domain and the total soil system (dimensionless). This approach is relatively complicated in that the model requires characterization of water retention and hydraulic conductivity functions (potentially of different form) for both pore regions, as well as a hydraulic conductivity function of the fracture–matrix interface. Note that the water contents,  $\theta_f$  and  $\theta_m$  in Eq. [4], have different meanings than in Eq. [3], where they represented water contents of the total pore space (i.e.,  $\theta = \theta_{mo} + \theta_{im}$ ), while here they refer to water contents of the two separate (fracture or matrix) pore domains such that

$$\theta = \theta_f + \theta_m = w\theta_f + (1-w)\theta_m$$
[5]

Hence, lowercase subscripts in the dual-permeability model refer to the local (pore-region) scale, while uppercase subscripts refer to the global (total soil medium) scale.

## Specific Models for Solute Transport

### Uniform Transport

Solute transport in numerical models is usually described using the relatively standard advection–dispersion equation (Fig. 1a and 2a) of the form

$$\frac{\partial \theta c}{\partial t} + \rho \frac{\partial s}{\partial t} = \frac{\partial}{\partial z} \left( \theta D \frac{\partial c}{\partial z} \right) - \frac{\partial qc}{\partial z} - \phi$$
[6]

or various extensions thereof (e.g., for two- and three-dimensional systems, or for multiple phases or components). In Eq. [6],  $c$  is the solution concentration [ $M L^{-3}$ ],  $s$  is the sorbed concentration [ $M M^{-1}$ ],  $D$  is the dispersion coefficient accounting for both molecular diffusion and hydrodynamic dispersion [ $L^2 T^{-1}$ ],  $q$  is the volumetric fluid flux density [ $L T^{-1}$ ] evaluated using the Darcy–Buckingham law, and  $\phi$  is a sink–source term that accounts for various zero- and first-order or other reactions [ $M L^{-3} T^{-1}$ ].

While HYDRUS-1D considers a general nonlinear sorption equation that can be simplified into a Langmuir or Freundlich isotherm (Šimůnek et al., 2005), for simplicity we assume here only linear adsorption of the form

$$s = K_d c$$
[7]

where  $K_d$  is the distribution coefficient [ $L^3 M^{-1}$ ]. Linear sorption leads to the following definition of the retardation factor  $R$  (dimensionless):

$$R = 1 + \frac{\rho K_d}{\theta}$$
[8]

In our examples below we will be using Eq. [7] for linear sorption and applying the resulting definition of  $R$  to all of the liquid domains involved (e.g., the total liquid phase, the mobile and immobile regions, or the matrix and macropore domains) with their appropriate parameters. Although considered in HYDRUS-1D, the effect of molecular diffusion will be neglected in the various examples. The dispersion coefficient  $D$  accounting only for hydrodynamic dispersion [ $L^2 T^{-1}$ ] is thus defined as

$$D = \lambda v = \lambda \frac{q}{\theta}$$
[9]

where  $\lambda$  is the dispersivity [ $L$ ] and  $v$  the average pore velocity [ $L T^{-1}$ ]. The same definition of the dispersion coefficient will be used for all mobile phases. HYDRUS-1D additionally considers molecular diffusion for transport in the gaseous phase, which will not be discussed here either. Finally, in the examples to follow we will use the time  $T$  needed to reach one pore volume of effluent. This time is given by

$$T = \frac{\theta L}{q}$$
[10]

where  $L$  is some distance (e.g., column length) within the transport domain being considered. For the physical nonequilibrium models discussed below, the pore volume for different domains is defined using corresponding water contents and fluxes.

### Physical Nonequilibrium Transport Models

#### Mobile–Immobile Water and Dual–Porosity Models

The concept of two-region, dual-porosity type solute transport (Fig. 1b, 1c, 2b, and 2c) was implemented already in earlier versions (1.0 and 2.0) of HYDRUS-1D to permit consideration of physical nonequilibrium transport. While the physical nonequilibrium transport model in the earlier versions was combined only with uniform water flow Eq. [1], Version 3.0 of HYDRUS-1D was expanded to also consider the dual-porosity water flow model Eq. [3] with a transient immobile water content. In both implementations, the governing solute transport equations are as follows:

$$\frac{\partial \theta_{mo} c_{mo}}{\partial t} + f_{mo} \rho \frac{\partial s_{mo}}{\partial t} = \frac{\partial}{\partial z} \left( \theta_{mo} D_{mo} \frac{\partial c_{mo}}{\partial z} \right) - \frac{\partial q_{mo} c_{mo}}{\partial z} - \phi_{mo} - \Gamma_s$$
[11a]

$$\frac{\partial \theta_{im} c_{im}}{\partial t} + (1 - f_{mo}) \rho \frac{\partial s_{im}}{\partial t} = \Gamma_s - \phi_{im}$$
[11b]

$$\Gamma_s = \omega_{mim} (c_{mo} - c_{im}) + \Gamma_w c^*$$
[11c]

in which solute exchange between the two liquid regions is modeled as the sum of an apparent first-order diffusion process and advective transport (where applicable). In Eq. [11],  $c_{mo}$  and  $c_{im}$  are concentrations of the mobile and immobile regions [ $M L^{-3}$ ], respectively;  $s_{mo}$  and  $s_{im}$  are sorbed concentrations of the mobile and immobile regions [ $M M^{-1}$ ], respectively;  $D_{mo}$  is the dispersion coefficient in the mobile region [ $L^2 T^{-1}$ ],  $q_{mo}$  is the volumetric fluid flux density in the mobile region [ $L T^{-1}$ ],  $\phi_{mo}$  and  $\phi_{im}$  are sink–source terms that account for various zero- and

first-order or other reactions in both regions [ $M L^{-3} T^{-1}$ ];  $f_{mo}$  is the fraction of sorption sites in contact with the mobile water content (dimensionless),  $\omega_{mim}$  is the mass transfer coefficient [ $T^{-1}$ ], and  $\Gamma_s$  is the mass transfer term for solutes between the mobile and immobile regions [ $M L^{-3} T^{-1}$ ]. Equation [11a] describes solute transport in the mobile (macropore) zone, Eq. [11b] is a mass balance for the immobile (micropore) domain, while Eq. [11c] ( $\Gamma_s$ ) describes the rate of mass transfer between the mobile and immobile domains. The second (advective) term of  $\Gamma_s$  in Eq. [11] is equal to zero for the Mobile–Immobile Model since that model does not consider water flow between the two regions. In the Dual-Porosity Model,  $c^*$  is equal to  $c_{mo}$  for  $\Gamma_w > 0$  and  $c_{im}$  for  $\Gamma_w < 0$ .

#### Dual-Permeability Model

Analogous to Eq. [4], the dual-permeability formulation for solute transport is based on advection–dispersion type equations for transport in both the fracture and matrix regions as follows (Gerke and van Genuchten, 1993a,b) (Fig. 1d and 2d):

$$\frac{\partial \theta_f c_f}{\partial t} + \rho \frac{\partial s_f}{\partial t} = \frac{\partial}{\partial z} \left( \theta_f D_f \frac{\partial c_f}{\partial z} \right) - \frac{\partial q_f c_f}{\partial z} - \phi_f - \frac{\Gamma_s}{w} \quad [12a]$$

$$\frac{\partial \theta_m c_m}{\partial t} + \rho \frac{\partial s_m}{\partial t} = \frac{\partial}{\partial z} \left( \theta_m D_m \frac{\partial c_m}{\partial z} \right) - \frac{\partial q_m c_m}{\partial z} - \phi_m + \frac{\Gamma_s}{1-w} \quad [12b]$$

$$\Gamma_s = \omega_{dp} (1-w) \theta_m (c_f - c_m) + \Gamma_w c^* \quad [12c]$$

The variables in Eq. [12] have similar meanings as in Eq. [11], except that they refer now to two overlapping domains, i.e., the matrix (subscript m) and fracture (subscript f) domains. Equation [12a] describes solute transport in the fracture domain, Eq. [12b] transport in the matrix domain, and Eq. [12c] advective–dispersive mass transfer between the fracture and matrix domains. Equation [12] assumes complete advective–dispersive transport descriptions for both the fractures and the matrix. Van Genuchten and Dalton (1986) and Gerke and van Genuchten (1996), among others, discussed possible expressions for the first-order solute mass transfer coefficient,  $\omega_{dp}$  [ $T^{-1}$ ].

#### Dual-Permeability Model with Immobile Water

The Dual-Permeability Model with Immobile Water (Fig. 1e and 2e) assumes that the liquid phase of the matrix can be further partitioned into mobile (flowing),  $\theta_{m,m}$  [ $L^3 L^{-3}$ ], and immobile (stagnant),  $\theta_{m,m}$  [ $L^3 L^{-3}$ ], regions as follows:

$$\theta_m = \theta_{m,m} + \theta_{im,m} \quad [13]$$

where  $\theta_m$  is the volumetric water content of the matrix pore system [ $L^3 L^{-3}$ ]. The governing advection–dispersion equation for transport in the matrix region (Eq. [12b]) is then replaced with the modified equations (Eq. [11]) (e.g., Pot et al., 2005) to yield

$$\frac{\partial \theta_f c_f}{\partial t} + \rho_f \frac{\partial s_f}{\partial t} = \frac{\partial}{\partial z} \left( \theta_f D_f \frac{\partial c_f}{\partial z} \right) - \frac{\partial q_f c_f}{\partial z} - \phi_f - \frac{\Gamma_s}{w} \quad [14a]$$

$$\frac{\partial \theta_{m,m} c_{m,m}}{\partial t} + \rho_m f_m \frac{\partial s_{m,m}}{\partial t} = \frac{\partial}{\partial z} \left( \theta_{m,m} D_m \frac{\partial c_{m,m}}{\partial z} \right) - \frac{\partial q_m c_{m,m}}{\partial z} - \phi_{m,m} + \frac{\Gamma_s}{1-w} - \Gamma_s^* \quad [14b]$$

$$\frac{\partial \theta_{im,m} c_{im,m}}{\partial t} + \rho_m (1-f_m) \frac{\partial s_{im,m}}{\partial t} = \Gamma_s^* - \phi_{im,m} \quad [14c]$$

$$\Gamma_s = \omega_{dp} (1-w) \theta_m (c_f - c_{m,m}) + \Gamma_w c^* \quad [14d]$$

$$\Gamma_s^* = \omega_{dpm} (c_{m,m} - c_{im,m}) \quad [14e]$$

where  $c_{im,m}$  and  $c_{m,m}$  are solute concentrations in the immobile and mobile zones of the matrix region [ $M L^{-3}$ ], respectively;  $\phi_{m,m}$  and  $\phi_{im,m}$  represent various reactions in the mobile and immobile parts of the matrix [ $M L^{-3} T^{-1}$ ], respectively;  $f_m$  is again the fraction of sorption sites in contact with the mobile region of the matrix (dimensionless),  $\omega_{dpm}$  is the mass transfer coefficient between mobile and immobile zones of the matrix region [ $T^{-1}$ ], and  $\Gamma_s^*$  is the mass transfer term for solutes between the mobile and immobile regions of the matrix domain [ $M L^{-3} T^{-1}$ ]. Equation [14a] now describes solute transport in the fracture domain, Eq. [14b] transport in the mobile zone of the matrix domain, Eq. [14c] is a mass balance for the immobile zone of the matrix domain, Eq. [14d] describes mass transfer between the fracture and matrix domains, while Eq. [14e] describes mass transfer between the mobile and immobile zones within the matrix domain.

### Chemical Nonequilibrium Transport Models

#### One Kinetic Site Model

When sorption in the Uniform Transport Model is considered (Fig. 3a) to be kinetic, Eq. [6] needs to be supplemented with an equation describing the kinetics of the sorption process. This is usually done by assuming a first-order process as follows:

$$\begin{aligned} \frac{\partial \theta c}{\partial t} + \rho \frac{\partial s^k}{\partial t} &= \frac{\partial}{\partial z} \left( \theta D \frac{\partial c}{\partial z} \right) - \frac{\partial qc}{\partial z} - \phi \\ \rho \frac{\partial s^k}{\partial t} &= \alpha_k \rho (s_e^k - s^k) - \phi_k \end{aligned} \quad [15]$$

$$s_e^k = K_d c$$

where  $s_e^k$  is the sorbed concentration that would be reached at equilibrium with the liquid-phase concentration [ $M M^{-1}$ ],  $s^k$  is the sorbed concentration of the kinetic sorption sites [ $M M^{-1}$ ],  $\alpha_k$  is a first-order rate constant describing the kinetics of the sorption process [ $T^{-1}$ ], and  $\phi_k$  represents a sink–source term that accounts for various zero- and first-order or other reactions at the kinetic sorption sites [ $M L^{-3} T^{-1}$ ].

#### Two-Site Model

Similarly to the mobile–immobile water concept, the concept of two-site sorption (Selim et al., 1976; van Genuchten and Wagenet, 1989) (Fig. 3b) was implemented already in Versions 1.0 and 2.0 of HYDRUS-1D to permit consideration of nonequilibrium adsorption–desorption reactions. The two-site sorption

concept assumes that the sorption sites can be divided into two fractions:

$$s = s^c + s^k \quad [16]$$

Sorption  $s^c$  [ $M M^{-1}$ ], on one fraction of the sites (Type 1 sites) is assumed to be instantaneous, while sorption  $s^k$  [ $M M^{-1}$ ], on the remaining (Type 2) sites is considered to be a first-order kinetic rate process. The system of equations describing the Two-Site Model is given by:

$$\frac{\partial \theta c}{\partial t} + \rho \frac{\partial s^c}{\partial t} + \rho \frac{\partial s^k}{\partial t} = \frac{\partial}{\partial z} \left( \theta D \frac{\partial c}{\partial z} \right) - \frac{\partial q c}{\partial z} - \phi \quad [17a]$$

$$s^c = f_c K_d c \quad [17b]$$

$$\rho \frac{\partial s^k}{\partial t} = \alpha_k \rho (s_c^k - s^k) - \phi_k \quad [17c]$$

$$s_c^k = (1 - f_c) K_d c \quad [17d]$$

where  $f_c$  is the fraction of exchange sites assumed to be in equilibrium with the liquid phase (dimensionless), and  $\alpha_k$  is a first-order rate constant [ $T^{-1}$ ]. Equation [17a] describes solute transport in the total system, Eq. [17b] equilibrium sorption onto the instantaneous sorption sites, Eq. [17c] is a mass balance of the kinetic sorption sites (van Genuchten and Wagenet, 1989), while Eq. [17d] represents the sorbed concentration of the kinetic sites when equilibrium would be reached with the liquid-phase concentration.

#### Two Kinetic Sites Model

To facilitate simulations of the transport of colloids or microorganisms (such as viruses and bacteria), Version 3.0 of HYDRUS-1D also implemented a Two Kinetic Sites Model (Fig. 3c) using the attachment–detachment approach:

$$\frac{\partial \theta c}{\partial t} + \rho \frac{\partial s_1^k}{\partial t} + \rho \frac{\partial s_2^k}{\partial t} = \frac{\partial}{\partial z} \left( \theta D \frac{\partial c}{\partial z} \right) - \frac{\partial q c}{\partial z} - \phi \quad [18]$$

$$\rho \frac{\partial s_1^k}{\partial t} = k_{a1} \theta c - k_{d1} \rho s_1^k - \phi_{k1}$$

$$\rho \frac{\partial s_2^k}{\partial t} = k_{a2} \theta c - k_{d2} \rho s_2^k - \phi_{k2}$$

where  $s_1^k$  and  $s_2^k$  are sorbed concentrations of the first and second fractions of kinetic sorption sites [ $M M^{-1}$ ], respectively;  $k_{a1}$  and  $k_{a2}$  are attachment coefficients for the first and second fractions of kinetic sorption sites [ $T^{-1}$ ], respectively;  $k_{d1}$  and  $k_{d2}$  are detachment coefficients for the first and second fractions of kinetic sorption sites [ $T^{-1}$ ], respectively; and  $\phi_{k1}$  and  $\phi_{k2}$  represent sink–source terms for the first and second fractions of kinetic sorption sites [ $M L^{-3} T^{-1}$ ], respectively. Note that the Two Kinetic Sites Model can be used (and often is used) to describe different processes. While the first kinetic process could be chemical attachment, the second kinetic process could represent physical straining (e.g., Bradford et al., 2004; Gargiulo et al., 2007, 2008). Note that in Eq. [18] we do not give the nonlinear blocking coefficients accounting for, for example, Langmuirian

blocking to attachment sites or depth-dependent straining that are considered in HYDRUS-1D (e.g., Bradford et al., 2004).

It is easily shown that the formulation based on attachment–detachment coefficients is mathematically identical to the formulation using first-order mass transfer coefficients. For example, by comparing Eq. [15] with [18] we have

$$\rho \frac{\partial s^k}{\partial t} = \theta k_a c - k_d \rho s^k = \rho \alpha_k (K_d c - s^k)$$

$$k_a = \alpha_k \frac{\rho}{\theta} K_d$$

$$k_d = \alpha_k$$

$$K_d = \frac{\theta k_a}{\rho \alpha_k}$$

[19]

#### Physical and Chemical Nonequilibrium Transport Models Dual-Porosity Model with One Kinetic Site

This model (Fig. 3d) is similar to the Dual-Porosity Model (Eq. [2]) in that the porous medium is divided into mobile and immobile domains such that  $\theta = \theta_{mo} + \theta_{im}$ . The current model, however, additionally divides the sorption sites in contact with the mobile zone, similarly to the Two-Site Model (Eq. [16]), into two fractions involving instantaneous and kinetic sorption such that the total sorption concentration at equilibrium is given by

$$\begin{aligned} s &= (1 - f_{mo}) s_{im} + f_{mo} s_{mo} \\ &= (1 - f_{mo}) s_{im} + f_{mo} (s_{mo}^c + s_{mo,e}^k) \\ &= (1 - f_{mo}) K_d c_{mo} + f_{mo} f_{em} K_d c_{mo} \\ &\quad + f_{mo} (1 - f_{em}) K_d c_{mo} \\ &= K_d c_{mo} \end{aligned} \quad [20]$$

where  $s_{mo}^c$  is the sorbed concentration in equilibrium with the liquid-phase concentration of the mobile region of the Dual-Porosity Model [ $M M^{-1}$ ],  $s_{mo,e}^k$  is the sorbed concentration of the kinetic sites in contact with the mobile region of the Dual-Porosity Model when at equilibrium [ $M M^{-1}$ ],  $f_{mo}$  is the fraction of sorption sites in contact with mobile water (the remainder is in contact with immobile water), and  $f_{em}$  is the fraction of sorption sites in equilibrium with the mobile liquid phase (the remaining kinetic sites are also in contact with the mobile liquid phase). The complete Dual-Porosity Model with One Kinetic Site is described using the following equations:

$$\frac{\partial \theta_{mo} c_{mo}}{\partial t} + f_{mo} \rho \frac{\partial s_{mo}^c}{\partial t} = \frac{\partial}{\partial z} \left( \theta_{mo} D_{mo} \frac{\partial c_{mo}}{\partial z} \right) - \frac{\partial q_{mo} c_{mo}}{\partial z} - \phi_{mo} - \Gamma_{s1} - \Gamma_{s2} \quad [21a]$$

$$\frac{\partial \theta_{im} c_{im}}{\partial t} + (1 - f_{mo}) \rho \frac{\partial s_{im}}{\partial t} = \Gamma_{s1} - \phi_{im} \quad [21b]$$

$$f_{mo} \rho \frac{\partial s_{mo}^k}{\partial t} = \Gamma_{s2} - \phi_{mo,k} \quad [21c]$$

$$\Gamma_{s1} = \omega_{ph} (c_{mo} - c_{im}) \quad [21d]$$

$$\Gamma_{s2} = \alpha_{ch}\rho (s_{mo,e}^k - s_{mo}^k) \quad [21e]$$

$$s_{mo}^e = f_{em}K_d c_{mo} \quad [21f]$$

$$s_{mo,e}^k = (1 - f_{em})K_d c_{mo} \quad [21g]$$

where  $\omega_{ph}$  and  $\alpha_{ch}$  are first-order rate constants [ $T^{-1}$ ] accounting for physical and chemical rate processes, respectively;  $\Gamma_{s1}$  is the mass transfer term for solute exchange between the mobile and immobile regions [ $M L^{-3} T^{-1}$ ];  $\Gamma_{s2}$  represents mass transfer to the kinetic sorption sites in the mobile region [ $M L^{-3} T^{-1}$ ]; and  $\phi_{mo}$ ,  $\phi_{im}$ , and  $\phi_{mo,k}$  represent sink–source terms for the equilibrium phases in the mobile zone, the immobile zone, and the kinetic sorption sites [ $M L^{-3} T^{-1}$ ], respectively. Equation [21a] describes transport in the mobile phase, Eq. [21b] is a mass balance for the immobile phase, and Eq. [21c] a mass balance for the kinetic sorption sites in contact with the mobile zone. Equations [21d] and [21e] describe mass transfer rates between the mobile and immobile zones and to the kinetic sorption sites, respectively, while Eq. [21f] and [21g] represent sorption onto the equilibrium and kinetic sorption sites in contact with the mobile zone, respectively.

#### Dual-Permeability Model with Two-Site Sorption

Finally, simultaneous physical and chemical nonequilibrium processes are implemented in HYDRUS-1D by assuming applicability of the Dual-Permeability Model (Gerke and van Genuchten, 1993a; Šimůnek et al., 2003) and dividing the sorption sites of both the fracture and matrix domains into equilibrium and kinetic sites (Fig. 3e). This model leads to the following set of equations (Pot et al., 2005):

$$\begin{aligned} \frac{\partial \theta_f c_f}{\partial t} + \rho_f \frac{\partial s_f^e}{\partial t} = \\ \frac{\partial}{\partial z} \left( \theta_f D_f \frac{\partial c_f}{\partial z} \right) - \frac{\partial q_f c_f}{\partial z} - \phi_f - \frac{\Gamma_s}{w} - \Gamma_f \\ \frac{\partial \theta_m c_m}{\partial t} + \rho_m \frac{\partial s_m^e}{\partial t} = \\ \frac{\partial}{\partial z} \left( \theta_m D_m \frac{\partial c_m}{\partial z} \right) - \frac{\partial q_m c_m}{\partial z} - \phi_m + \frac{\Gamma_s}{1-w} - \Gamma_m \end{aligned} \quad [22]$$

$$\rho \frac{\partial s_f^k}{\partial t} = \Gamma_f - \phi_{f,k}$$

$$\rho \frac{\partial s_m^k}{\partial t} = \Gamma_m - \phi_{m,k}$$

$$\Gamma_s = \omega_{dp} (1-w) \theta_m (c_f - c_m) + \Gamma_w c^*$$

$$\Gamma_f = \rho_f \alpha_{ch,f} \left[ (1 - f_f) K_{df} c_f - s_f^k \right]$$

$$\Gamma_m = \rho_m \alpha_{ch,m} \left[ (1 - f_m) K_{dm} c_m - s_m^k \right]$$

where  $s_m^k$  and  $s_f^k$  are sorbed concentrations of Type 2 (kinetic) sites in the matrix and fracture domains [ $M M^{-1}$ ], respectively;  $f_m$  and  $f_f$  are fractions of the exchange sites assumed to be in equilibrium with the solution phases (dimensionless) of the

matrix and fracture domains, respectively;  $\phi_f$ ,  $\phi_m$ ,  $\phi_{f,k}$ , and  $\phi_{m,k}$  represent reactions in the equilibrium phases of the fracture and matrix domains and at the kinetic sites of the fracture and matrix domains [ $M L^{-3} T^{-1}$ ], respectively; and  $\alpha_{ch,m}$  and  $\alpha_{ch,f}$  are again first-order rate constants for the matrix and fracture domains [ $T^{-1}$ ], respectively. Note that the distribution coefficients can be different in the different regions (i.e.,  $K_{df} \neq K_{dm}$ ).

## Numerical Implementation

All of the models presented here were implemented in the HYDRUS-1D software package and as such are all solved with very similar numerical techniques. The Galerkin-type linear finite element method was used for spatial discretization of the governing partial differential equations, while finite difference methods were used to approximate temporal derivatives. A fully implicit finite difference scheme with Picard linearization was used to solve the Richards equation, while a Crank–Nicholson finite difference scheme was used for solution of the advection–dispersion equations. For the dual-permeability models, we always first solved the equations describing processes in the matrix, after which the equations describing processes in the fractures were solved. Complete details about the invoked numerical techniques are provided in the HYDRUS-1D technical manual (Šimůnek et al., 2008).

## Implications for Formulation of the Inverse Problem

The physical and chemical nonequilibrium models both involve relatively large numbers of parameters, many of which cannot be (or cannot easily be) measured independently. Some parameters need to be obtained by calibrating a particular model against laboratory or field measurements. This is usually done using a parameter estimation procedure (e.g., Šimůnek and Hopmans, 2002; Šimůnek et al., 2002) in which the sum of squared deviations between measurements and model predictions, organized in an objective function, is minimized. While the definition of the objective function for models that consider only uniform flow and transport may be relatively straightforward, the objective functions for calibration of the nonequilibrium models can become extremely complicated. For the equilibrium flow and transport models, one usually defines the objective function in terms of measured pressure heads, water contents, solution concentrations, or actual or cumulative water or solute fluxes. Note from Fig. 1a that the system is always described using unique values of the water content, pressure head, or solution concentration. In addition to the resident concentration, the objective function can also be defined using the flux concentration or the total solute mass at a specified location. The total solute mass must include not only the mass in the liquid phase but also the mass sorbed to either instantaneous or kinetic sorption sites (the latter if a kinetic sorption model is used).

By comparison, when physical nonequilibrium models are used, one can encounter different water contents such as the mobile water content, the immobile water content, the water content of the fracture domain, the water content of the matrix, or the total water content. The nonequilibrium models typically will also involve different types of concentrations, including concentrations of the mobile and immobile zones, sorbed concentrations



associated with instantaneous and kinetic sorption sites, and total concentrations. Since different measurement techniques may lead to different types of concentrations (e.g., resident, flux, or total concentrations), a flexible inverse approach should also allow for the different modes of concentrations. Different types of water and solute fluxes can furthermore be defined in the nonequilibrium models, including total fluxes, fluxes in the mobile zone, or fluxes in the fracture and matrix domains. To provide users with flexibility during the model calibration process, these various water contents, concentrations, and water and solute fluxes must be considered in the objective function. Table 2 provides a list of variables in the different equilibrium and nonequilibrium models that can be incorporated in the objective function when HYDRUS-1D is used for parameter estimation purposes.

## Applications

We now briefly demonstrate the main features of selected transport models, including especially the sensitivity of calculated breakthrough curves to several key transport parameters. As before, we will focus only on solute transport, while assuming that water flow is at full saturation and steady state and thus that the various water contents and fluxes are constant with depth and time. Steady-state flow is initiated by fixing all pressure heads in the system equal to zero (both the initial and boundary conditions).

### Uniform Transport

The uniform (equilibrium) solute transport model during steady-state water flow is fully defined in terms of four parameters (Table 1). Of these, two parameters (the water content,  $\theta$ , and the fluid flux density,  $q$ ) are related to water flow, and only two parameters (the dispersivity,  $\lambda$ , and the distribution coefficient,  $K_d$ ) are directly related to solute transport. Figure 4 shows the well-known effects of the dispersivity (left) and the distribution coefficient (right) on calculated breakthrough curves. Notice that the red lines in Fig. 4 (left and right) represent the same simulation. While higher values of the dispersivity lead to earlier arrival of the solute and more pronounced tailing compared with lower  $\lambda$  values, larger values of the distribution coefficient delay the arrival of solute in the effluent. Note that the selected distribution coefficients of 0, 1, and 3 lead to retardation factors of 1, 4, and 10, respectively. Also note that one pore volume (Eq. [10]) for the selected parameters corresponds to 1 d.

### Physical Nonequilibrium Transport Models

#### Mobile–Immobile Water and Dual-Porosity Models

Since the immobile water content is constant for conditions of steady-state water flow for both the Mobile–Immobile Water and the Dual-Porosity models, the two models are identical with respect to solute transport. These two models have three additional parameters compared with the Uniform Transport Model: the immobile water content ( $\theta_{im}$ ), the fraction of sorption sites in contact with mobile water ( $f_{mo}$ ), and the mass transfer coefficient ( $\omega_{mim}$ ) (Table 1). Figure 5 demonstrates the effect of the mass transfer coefficient (left) and the fraction of mobile water (right) on calculated breakthrough curves. For the breakthrough curves in Fig. 5 (left), one pore volume ( $T = L\theta_{mo}/q$ ) is equal to 1 d and the retardation factor of the mobile phase ( $R = 1 + f_{mo}\rho K_d/\theta_{mo}$ ) is equal to 4. Notice that the effluent concentration for the case with the lowest value of the mass transfer coefficient ( $0.1 \text{ d}^{-1}$ ), i.e.,

the case most resembling uniform transport in the mobile region, indeed reaches approximately 0.5 after about 4 d. Notice also that this breakthrough curve shows the most tailing resulting from the slow release of solute from the mobile zone into immobile liquid. The large value of the mass transfer coefficient ( $10 \text{ d}^{-1}$ ) leads to fast equilibration of the concentrations of the mobile and immobile zones, and thus to a breakthrough curve resembling uniform transport in the entire pore system ( $T = 1.666 \text{ d}$  and  $R = 4$ ) characterized by a relatively sigmoidal curve. If the mass transfer coefficient had been equal to zero (i.e., equilibrium flow in the mobile region), the resulting breakthrough curves would have been the same as in Fig. 4. Figure 5 (right) demonstrates the effect of an increasing fraction of immobile water and the corresponding fraction of sorption sites. Following Nkedi-Kizza et al. (1983), the ratios of mobile to total water ( $\theta_{mo}/\theta$ ) and equilibrium to total sorption sites ( $f$ ) were assumed to be the same. A smaller fraction of mobile water leads to earlier solute arrival and more pronounced tailing. Notice that the red lines in Fig. 5 (left and right) represent the same simulation.

#### Dual-Permeability Model

In the dual-permeability system, solute moves simultaneously through two overlapping porous regions, with the number of model parameters further increasing. Solute transport during steady-state water flow now requires the following nine parameters: two water contents ( $\theta_m$  and  $\theta_f$ ), two fluxes ( $q_m$  and  $q_f$ ), two dispersivities ( $\lambda_m$  and  $\lambda_f$ ), distribution coefficients for each domain ( $K_{dm}$  and  $K_{df}$ ), and a mass transfer coefficient  $\omega_{dp}$ . The exchange of solute between the two pore regions is proportional to the mass transfer coefficient  $\omega_{dp}$ . When this coefficient is equal to zero (black lines in Fig. 6), solute will move independently through each of the two pore systems, in which case the transport process reduces to that of the uniform transport model applied separately to each of the two pore systems. Outflow concentrations from the matrix (thin line), fracture (intermediate line), and the entire soil (thick line) are shown in Fig. 6. Note that due to accelerated transport in the dual-permeability system, the time scale in Fig. 6 is only 10 d, compared with 20 d in the preceding examples. For the selected parameters, the retardation factor for both regions is equal to 4 and the pore volumes are equal to 0.1666 and 1.666 d for the fracture and matrix domains, respectively. The solute front indeed arrives after about 0.6666 and 6.666 d ( $TR$ ) in the fracture and matrix domains, respectively. The average outflow concentration can now be obtained as a weighted average of the outflow concentrations from each domain:

$$c_T = \frac{wc_f q_f + (1-w)c_m q_m}{w q_f + (1-w) q_m} \quad [23]$$

As shown in Fig. 6, the average outflow concentration quickly increases initially, similarly as for the fracture domain, but then stabilizes at about 0.5 since only about half of the outflow comes from the fracture domain. When solute arrives also in the outflow from the matrix domain, the average outflow concentration gradually increases again until it reaches unit concentration. The solute breakthrough curves start deviating from those calculated using the Uniform Flow Model individually for the matrix and macropore regions when the mass transfer coefficient is increased (red lines in Fig. 6) because of exchange of solute between the two regions. For relatively large values of the mass transfer coefficient, this causes

TABLE 2. Variables that can be included in the objective function.

Model	Variable	Definition
Uniform model	Water content	$\theta$
	Pressure head	$h$
	Resident concentration	$c$
	Flux concentration	$c - \frac{D\theta}{q} \frac{\partial c}{\partial z}$
	Total solute mass (uniform transport)	$c(\theta + \rho K_d)$
	Total solute mass (One Kinetic Site Model)	$c\theta + \rho s^k$
	Total solute mass (Two-Site Model)	$c(\theta + f_e \rho K_d) + \rho s^k$
	Total solute mass (Two Kinetic Sites Model)	$c\theta + \rho s_1^k + \rho s_2^k$
Dual-Porosity	Water content	$\theta = \theta_{mo} + \theta_{im}$
	Pressure head	$h_{mo}$
	Mobile-zone resident concentration	$c_{mo}$
	Immobile-zone resident concentration	$c_{im}$
	Mobile-zone flux concentration	$c_{mo} - \frac{D_{mo}\theta_{mo}}{q_{mo}} \frac{\partial c_{mo}}{\partial z}$
	Average liquid concentration	$c_{TI} = \frac{c_{mo}\theta_{mo} + c_{im}\theta_{im}}{\theta}$
	Total solute mass (no chemical nonequilibrium)	$c_{mo}(\theta_{mo} + f_{mo}\rho K_d) + c_{im}[\theta_{im} + (1 - f_{mo})\rho K_d]$
	Total solute mass (kinetic sorption)	$c_{mo}(\theta_{mo} + f_{mo}f_{em}\rho K_d) + f_{mo}\rho s_{mo}^k + c_{im}[\theta_{im} + (1 - f_{mo})\rho K_d]$
Dual-Permeability	Matrix water content	$\theta_M = (1 - w)\theta_m$
	Fracture water content	$\theta_F = w\theta_f$
	Total water content	$\theta = w\theta_f + (1 - w)\theta_m$
	Matrix pressure head	$h_m$
	Fracture pressure head	$h_f$
	Matrix flux	$q_m(1 - w)$
	Fracture flux	$q_f w$
	Total flux	$q_m(1 - w) + q_f w$
	Fracture concentration	$c_f$
	Matrix concentration	$c_m$
	Flux concentration	$\frac{w c_f q_f + (1 - w) c_m q_m}{w q_f + (1 - w) q_m}$
	Average liquid concentration	$\frac{w c_f \theta_f + (1 - w) c_m \theta_m}{w \theta_f + (1 - w) \theta_m}$
	Total solute mass (no chemical nonequilibrium)	$w c_f (\theta_f + \rho_f K_{df}) + (1 - w) c_m (\theta_m + \rho_m K_{dm})$
	Total solute mass (kinetic sorption)	$w [c_f (\theta_f + f_f \rho_f K_{df}) + \rho_f s_f^k] + (1 - w) [c_m (\theta_m + f_m \rho_m K_{dm}) + \rho_m s_m^k]$
Dual-Permeability with MIM	Matrix water content	$\theta_M = (1 - w)(\theta_{m,m} + \theta_{im,m})$
	Fracture water content	$\theta_F = w\theta_f$
	Total water content	$\theta = w\theta_f + (1 - w)(\theta_{m,m} + \theta_{im,m})$
	Matrix pressure head	$h_m$
	Fracture pressure head	$h_f$
	Matrix flux	$q_m(1 - w)$
	Fracture flux	$q_f w$
	Total flux	$q_m(1 - w) + q_f w$
	Fracture concentration	$c_f$
	Matrix immobile concentration	$c_{im,m}$
	Matrix mobile concentration	$c_{m,m}$
	Flux concentration	$\frac{w c_f q_f + (1 - w) c_{m,m} q_m}{w q_f + (1 - w) q_m}$
	Average liquid concentration	$\frac{w c_f \theta_f + (1 - w) (c_{m,m} \theta_{m,m} + c_{im,m} \theta_{im,m})}{w \theta_f + (1 - w) (\theta_{m,m} + \theta_{im,m})}$
	Total solute mass (no chemical nonequilibrium)	$w c_f (\theta_f + \rho_f K_{df}) + (1 - w) [c_{m,m} (\theta_{m,m} + f_{m,m} \rho_m K_{dm}) + c_{im,m} (\theta_{im,m} + (1 - f_{m,m}) \rho_m K_{dm})]$

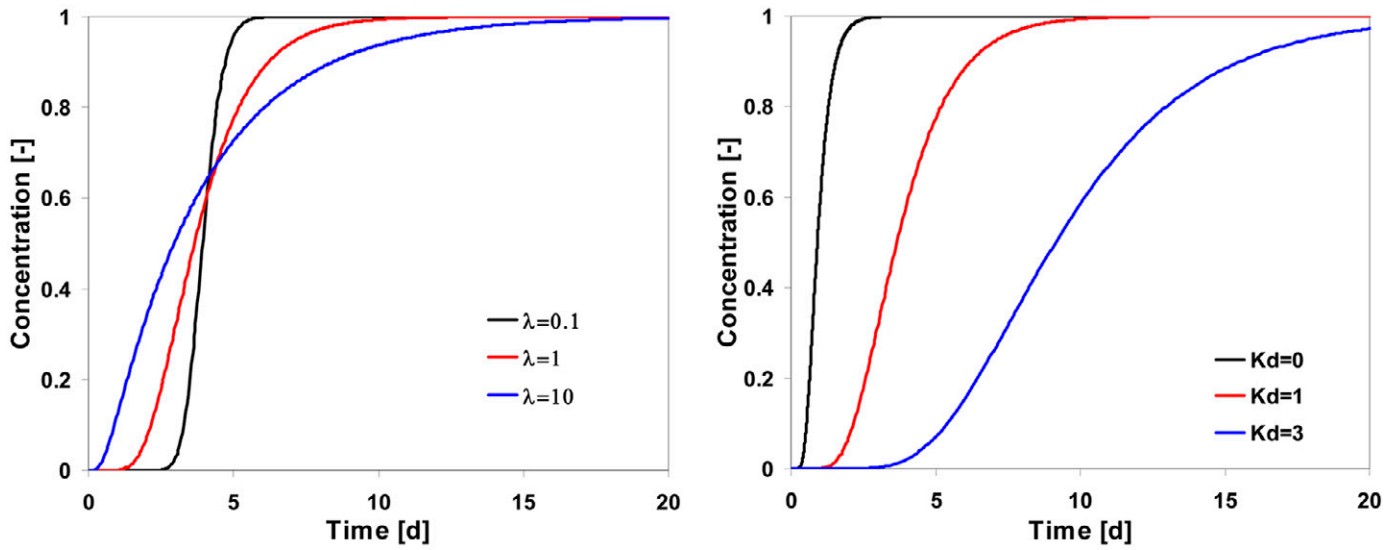


FIG. 4. Breakthrough curves calculated using the Uniform Transport Model for a 10-cm-long soil column and the following parameters:  $q = 5 \text{ cm d}^{-1}$ ,  $\theta = 0.5$ , and  $\rho_b = 1.5 \text{ g cm}^{-3}$ ; on the left,  $K_d = 1 \text{ cm}^3 \text{ g}^{-1}$  and  $\lambda = 0.1, 1, \text{ and } 10 \text{ cm}$ ; and on the right,  $\lambda = 1 \text{ cm}$  and  $K_d = 0, 1, \text{ and } 3 \text{ cm}^3 \text{ g}^{-1}$ .

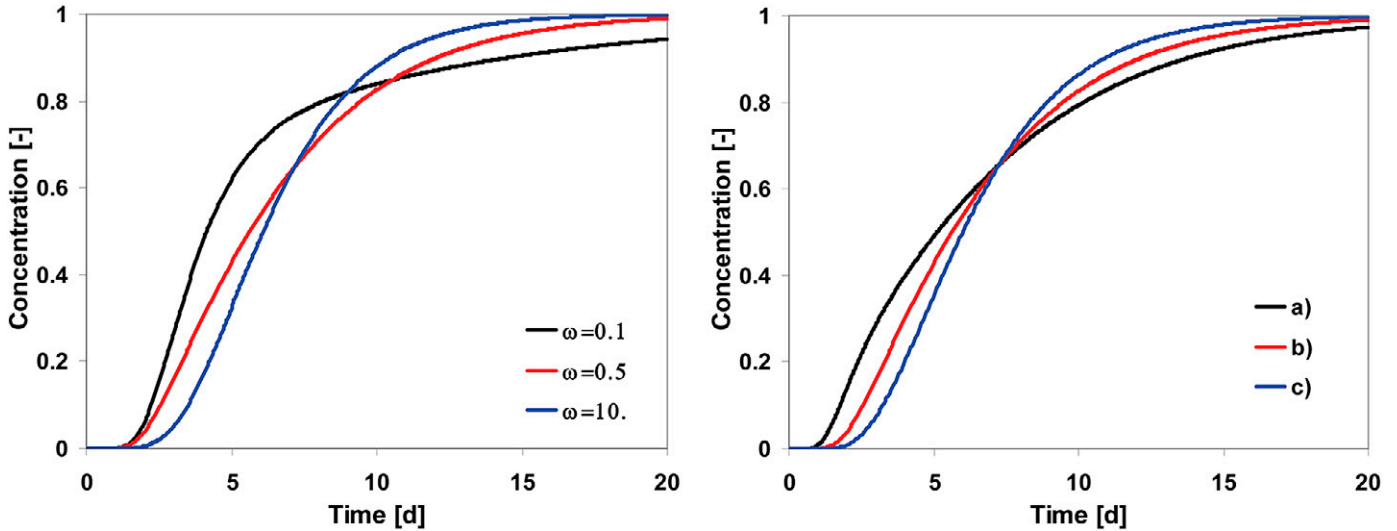


FIG. 5. Breakthrough curves calculated using the Mobile-Immobile Water Model for a 10-cm-long soil column and the following parameters:  $q = 3 \text{ cm d}^{-1}$ ,  $\theta = 0.5$ ,  $\lambda_{mo} = 1 \text{ cm}$ ,  $K_d = 1 \text{ cm}^3 \text{ g}^{-1}$ ,  $\rho_b = 1.5 \text{ g cm}^{-3}$ . On the left:  $f_{mo} = 0.6$ ,  $\theta_{mo} = 0.3$ ,  $\theta_{im} = 0.2$ , and  $\omega_{mim} = 0.1, 0.5, 10 \text{ d}^{-1}$ . On the right:  $\omega_{mim} = 0.5 \text{ d}^{-1}$  and (a)  $f_{mo} = 0.4$ ,  $\theta_{mo} = 0.2$ ,  $\theta_{im} = 0.3$ ; (b)  $f_{mo} = 0.6$ ,  $\theta_{mo} = 0.3$ ,  $\theta_{im} = 0.2$ ; and (c)  $f_{mo} = 0.8$ ,  $\theta_{mo} = 0.4$ ,  $\theta_{im} = 0.1$ .

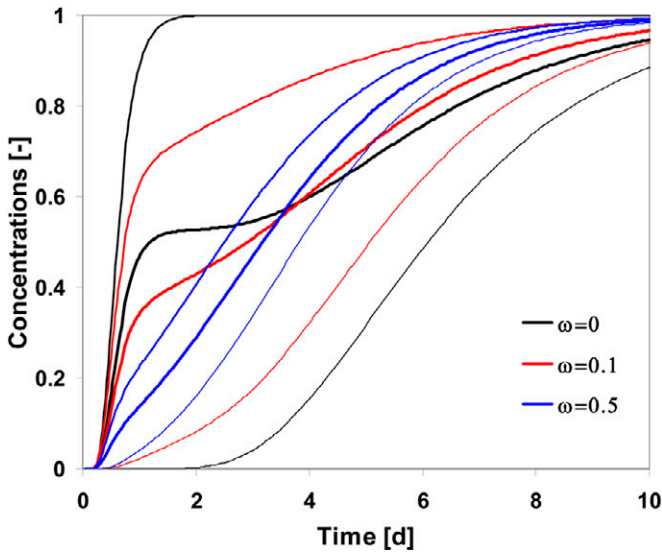


FIG. 6. Breakthrough curves calculated using the Dual-Permeability Model for a 10-cm-long soil column and the following parameters:  $q_m = 3 \text{ cm d}^{-1}$ ,  $q_f = 30 \text{ cm d}^{-1}$ ,  $\theta = \theta_m = \theta_f = 0.5$ ,  $w = 0.1$ ,  $\lambda_m = \lambda_f = 1 \text{ cm}$ ,  $K_{dm} = K_{df} = 1 \text{ cm}^3 \text{ g}^{-1}$ ,  $\rho_b = 1.5 \text{ g cm}^{-3}$ , and  $\omega_{dp} = 0, 0.1, \text{ and } 0.5 \text{ d}^{-1}$ . Matrix, fracture, and total breakthrough curves are represented by thin, medium, and thick lines, respectively.

rapid equilibration of the concentrations of the two domains. The breakthrough curves from the two regions will then start converging and will again resemble the results of the uniform transport model applied to the entire soil (blue lines in Fig. 6). For a fully equilibrated system,  $R$  equals 4 and one pore volume equals 0.88 d, causing the solute to arrive at approximately 3.5 d.

#### Dual-Permeability with Mobile–Immobile Water Model

The simulations above (red lines in Fig. 6) were further modified by assuming the presence of immobile water (varying between water contents of 0 and 0.4) and a corresponding fraction of sorption sites in the matrix region. The resulting model requires three additional parameters: the immobile water content of the matrix domain ( $\theta_{im,m}$ ), the fraction of sorption sites in contact with the mobile zone of the matrix domain ( $f_m$ ), and the mass transfer coefficient characterizing solute exchange between the mobile and immobile zones of the matrix domain ( $\alpha_k$ ). Since the same flux is forced through an increasingly smaller part of the matrix domain, the average pore water velocity increases and solute in the matrix region will arrive earlier at the end of the column (Fig. 7). Increased concentrations in the mobile zone of the matrix domain lead to smaller gradients between the fracture and matrix domains, and correspondingly less solute exchange between the two domains. This, in turn, causes less tailing in the breakthrough curve of the fracture domain. When only 20% of water in the matrix domain is mobile ( $\theta_m = 0.5$ ,  $\theta_{im,m} = 0.1$ ,  $\theta_{m,m} = 0.4$ ), the average pore water velocity is only half of that in the fracture domain (green lines in Fig. 7).

#### Chemical Nonequilibrium Transport Models

##### One Kinetic Site Model

The simulation of Fig. 4 (red, uniform transport) was taken as a basis for evaluating the effect of kinetic sorption. Compared with the Uniform Flow Model, the One Kinetic Site Model

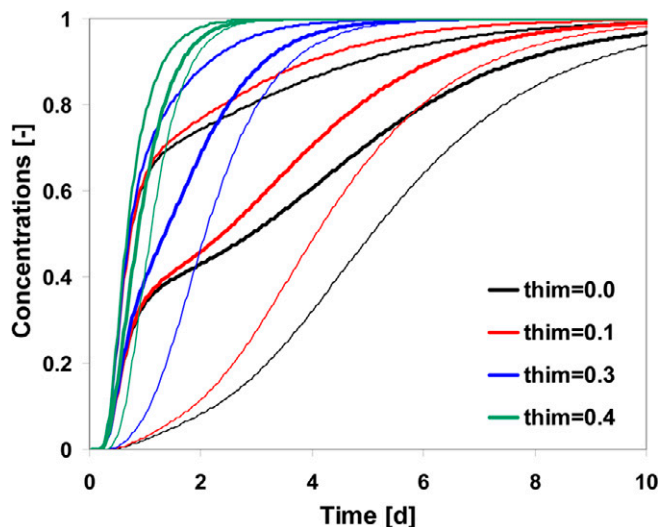


FIG. 7. Breakthrough curves calculated using the Dual-Permeability Model with MIIM for a 10-cm-long soil column and the following parameters:  $q_m = 3 \text{ cm d}^{-1}$ ,  $q_f = 30 \text{ cm d}^{-1}$ ,  $\theta = \theta_m = \theta_f = 0.5$ ,  $w = 0.1$ ,  $\lambda_m = \lambda_f = 1 \text{ cm}$ ,  $K_{dm} = K_{df} = 1 \text{ cm}^3 \text{ g}^{-1}$ ,  $\rho_b = 1.5 \text{ g cm}^{-3}$ ,  $\omega_{dp} = 0.1 \text{ d}^{-1}$ ,  $\omega_{dpm} = 0.1 \text{ d}^{-1}$ ,  $\theta_{im,m}$  (thim) = 0.0, 0.1, 0.3, and 0.4, and  $f_m = 1, 0.8, 0.4$ , and 0.2, respectively. Matrix, fracture, and total breakthrough curves are represented by thin, medium, and thick lines, respectively.

requires only one additional parameter: the mass transfer coefficient  $\alpha_k$  characterizing the sorption process. Three different values for  $\alpha_k$  of 0.1, 0.5, and  $10 \text{ d}^{-1}$  were considered. The larger value of the mass transfer coefficient ( $\alpha_k = 10 \text{ d}^{-1}$ ) leads to relatively fast equilibration between the liquid- and solid-phase concentrations, and therefore to a relatively sigmoidal breakthrough curve (blue line in Fig. 8) resembling uniform transport (red line in Fig. 4). Lower values of the mass transfer coefficient lead to less sorption because of slower equilibration between the liquid and solid phases, and consequently to earlier solute arrival and more pronounced tailing (black line in Fig. 8).

##### Two-Site Model

The same simulations as for the One Kinetic Site Model were repeated with the Two-Site Model, assuming that 40% of the sorption sites were in equilibrium with the liquid-phase concentrations (Fig. 9, left). This model, compared with the One Kinetic Site Model, requires only one additional parameter: the fraction of sorption sites ( $f_c$ ) in equilibrium with the liquid-phase concentration. The effect on the breakthrough curve obtained with a mass transfer coefficient,  $\alpha_k$ , of  $10 \text{ d}^{-1}$  was relatively small since this value by itself represents rapid sorption. Other breakthrough curves deviated less from this simulation than for the One Kinetic Site Model because of the relatively high fraction of sorption sites that were at equilibrium with the liquid phase. Similarly to the One Kinetic Site Model, smaller values of the mass transfer coefficient caused earlier solute arrival and more prolonged tailing, but to a lesser extent. Figure 9 (right) demonstrates the effect of the fraction of sorption sites in equilibrium with the liquid phase on the computed breakthrough curves. The red lines in Fig. 9 (left and right) again represent the same simulation. A smaller fraction of sorption sites in equilibrium with the liquid phase leads to less instantaneous sorption, more kinetic sorption, and more pronounced tailing, and thus correspondingly to earlier solute arrival than when a larger fraction of instantaneous sites is considered.

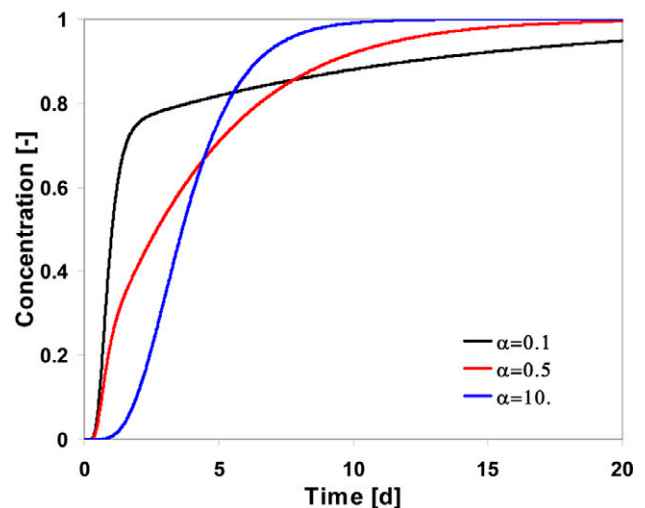


FIG. 8. Breakthrough curves calculated using the One Kinetic Site Model for a 10-cm-long soil column and the following parameters:  $q = 5 \text{ cm d}^{-1}$ ,  $\theta = 0.5$ ,  $\lambda = 1 \text{ cm}$ ,  $K_d = 1 \text{ cm}^3 \text{ g}^{-1}$ ,  $\rho_b = 1.5 \text{ g cm}^{-3}$ , and  $\alpha_k = 0.1, 0.5$ , and  $10 \text{ d}^{-1}$ .

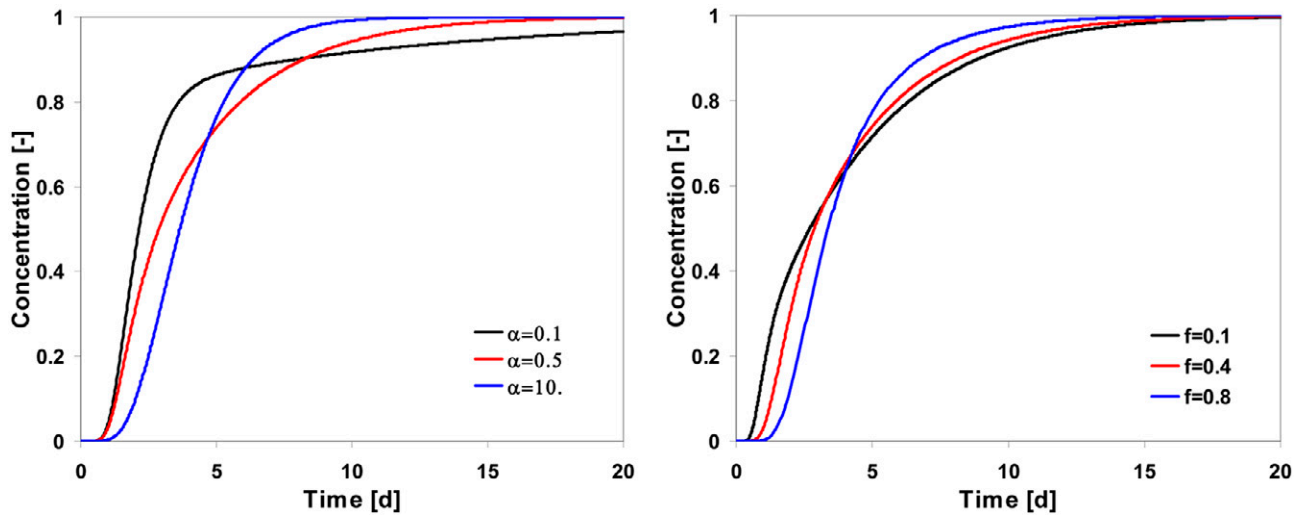


FIG. 9. Breakthrough curves calculated using the Two-Site Kinetic Model for a 10-cm-long soil column and the following parameters:  $q = 5 \text{ cm d}^{-1}$ ,  $\theta = 0.5$ ,  $\lambda = 1 \text{ cm}$ ,  $K_d = 1 \text{ cm}^3 \text{ g}^{-1}$ , and  $\rho_b = 1.5 \text{ g cm}^{-3}$ ; on the left,  $f_e = 0.4$  and  $\alpha_k = 0.1, 0.5,$  and  $10 \text{ d}^{-1}$ ; and on the right,  $\alpha_k = 0.5 \text{ d}^{-1}$  and  $f_e = 0.1, 0.4,$  and  $0.8$ .

#### Two Kinetic Sites Model

The colloid attachment–detachment model has the same number of parameters as the One Kinetic Site Model, except that the parameters  $K_d$  and  $\alpha_k$  are replaced with attachment ( $k_a$ ) and detachment ( $k_d$ ) coefficients. Since we considered two different sorption sites, we have two pairs of attachment and detachment coefficients ( $k_{a1}, k_{d1}, k_{a2}, k_{d2}$ ). Here we used Eq. [19] to convert the One-Site Kinetic Model parameters ( $K_d = 1 \text{ cm}^3 \text{ g}^{-1}$ ,  $\alpha_k = 0.5 \text{ d}^{-1}$ ; red line in Fig. 8) into attachment–detachment coefficients ( $k_{a1} = 1.5 \text{ d}^{-1}$ ,  $k_{d1} = 0.5 \text{ d}^{-1}$ ) for the first fraction of sorption sites. Additionally, a finite (10-d) duration of the solute pulse was considered, while varying the attachment–detachment coefficients ( $k_{a2}$  and  $k_{d2}$ , respectively) for the second fraction of sorption sites. In the remaining examples, a finite solute pulse is used so that both increasing and decreasing limbs of the breakthrough curves can be displayed. Increased attachment to and detachment from the second fraction of sorption sites reduced the outflow concentrations during the first part of the breakthrough curves, but increased them during the second part (Fig. 10).

#### Physical and Chemical Nonequilibrium Flow and Transport Models Dual-Porosity Model with One Kinetic Site

Compared with the Dual-Porosity Model, this model has two additional parameters characterizing kinetic sorption in the mobile zone, i.e., the fraction of sorption sites ( $f_{em}$ ) in equilibrium with the liquid-phase concentration of the mobile zone, and the mass transfer coefficient ( $\alpha_{ch}$ ). The simulations in Fig. 5 obtained with the Dual-Porosity Model were modified by assuming the presence of kinetic sorption sites in the mobile zone. We first assumed that 40% of the sorption sites in the mobile phase ( $f_{em} = 0.4$ ) was at equilibrium with the mobile liquid phase and that the remaining sites were kinetic, using mass transfer coefficients,  $\alpha_{ch}$ , of 0.1, 0.5, and  $10 \text{ d}^{-1}$  (Fig. 11, left). We next assumed that  $\alpha_{ch}$  was constant and equal to  $0.1 \text{ d}^{-1}$  while the fraction of sorption sites in the mobile phase at equilibrium with the liquid concentration of the mobile water varied ( $f_{em} = 0.1, 0.4, 0.7,$  and  $1$ ) (Fig. 11, right). We further assumed in both sets of simulations that the duration of the solute pulse was 10 d. Notice

that the red lines in Fig. 11 (left and right) again represent the same simulation. Results presented in Fig. 11 (left) display the same characteristics as results shown in Fig. 9 for the Two Site Kinetic Model. Lower values of the mass transfer coefficient lead to less sorption because of slower equilibration between the liquid and solid phases, and hence to earlier solute arrival and more pronounced tailing (black line in Fig. 11, left). A smaller fraction of sorption sites in equilibrium with the liquid phase leads to less instantaneous sorption and more kinetic sorption, and hence to earlier solute arrival than when a larger fraction of instantaneous sites is considered (Fig. 11, right).

#### Dual-Permeability Model with Two-Site Sorption

This model, compared with the Dual-Permeability Model, has four additional parameters characterizing kinetic sorption in both regions, i.e., the fractions of sorption sites in equilibrium with the liquid-phase concentrations of both regions ( $f_m$  and  $f_r$ )

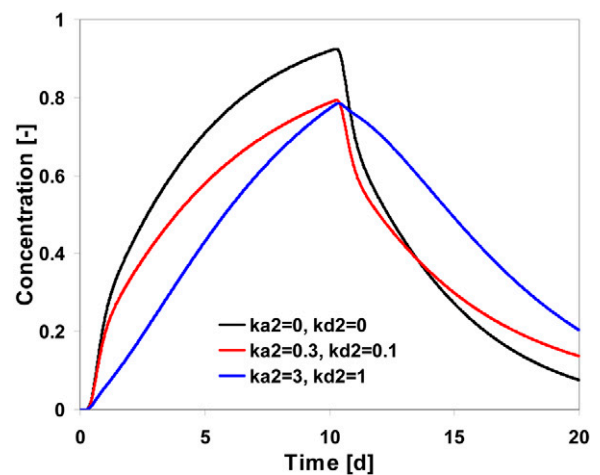


FIG. 10. Breakthrough curves calculated using the Two Kinetic Sites Model for a 10-cm-long soil column and the following parameters: solute pulse duration = 10 d,  $q = 5 \text{ cm d}^{-1}$ ,  $\theta = 0.5$ ,  $\lambda = 1 \text{ cm}$ ,  $K_d = 1 \text{ cm}^3 \text{ g}^{-1}$ ,  $\rho_b = 1.5 \text{ g cm}^{-3}$ ,  $k_{a1} = 1.5 \text{ d}^{-1}$ ,  $k_{d1} = 0.5 \text{ d}^{-1}$ , and  $k_{a2} = 0.0, 0.3,$  and  $3.0 \text{ d}^{-1}$  with  $k_{d2} = 0.0, 0.1,$  and  $1.0 \text{ d}^{-1}$ , respectively.

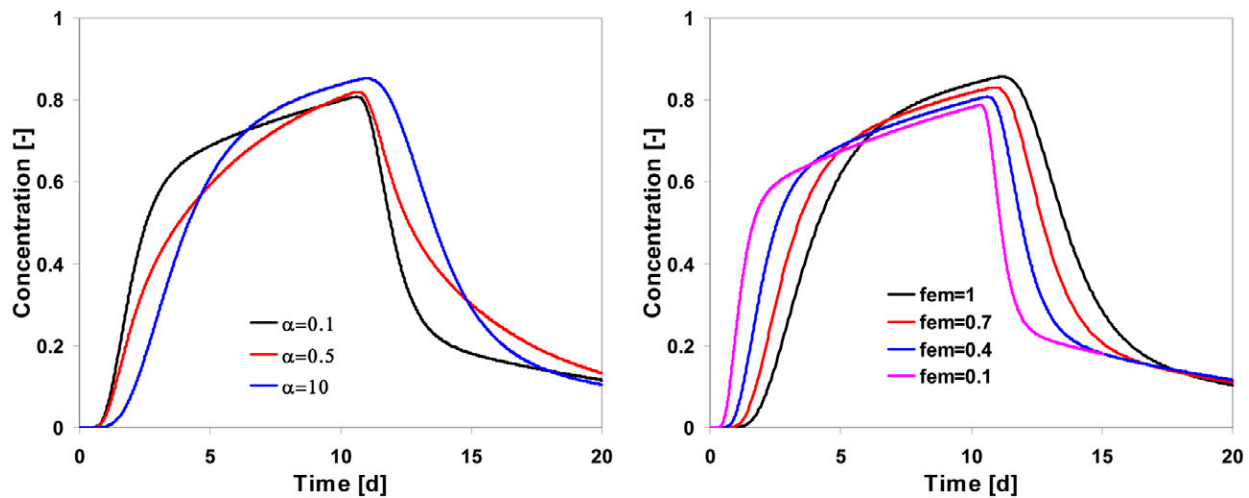


FIG. 11. Breakthrough curves calculated using the Dual-Porosity Model with One Kinetic Site for a 10-cm-long soil column and the following parameters: solute pulse duration = 10 d,  $q = 3 \text{ cm d}^{-1}$ ,  $\theta = 0.5$ ,  $\theta_{mo} = 0.3$ ,  $\theta_{im} = 0.2$ ,  $\lambda_{mo} = 1 \text{ cm}$ ,  $K_d = 1 \text{ cm}^3 \text{ g}^{-1}$ ,  $\rho_b = 1.5 \text{ g cm}^{-3}$ ,  $f_{mo} = 0.6$ ,  $\alpha = 0.1 \text{ d}^{-1}$ ; on the left,  $f_{em} = 0.4$  and  $\alpha_{ch} = 0.1, 0.5,$  and  $10 \text{ d}^{-1}$ ; and on the right,  $\alpha_{ch} = 0.1 \text{ d}^{-1}$  and  $f_{em} = 1.0, 0.7, 0.4,$  and  $0.1$ .

and the mass transfer coefficients for both regions ( $\alpha_{ch,m}$  and  $\alpha_{ch,f}$ ). The simulation in Fig. 6 (red line) with a mass transfer coefficient,  $\omega_{dp}$ , of  $0.1 \text{ d}^{-1}$  was recalculated assuming the presence of kinetic and equilibrium sorption sites in both the matrix and fracture domains, and using a finite duration (10 d) of the applied solute pulse (Fig. 12). Outflow concentrations from the matrix (thin line), the fracture domain (intermediate line), and the entire soil (thick line) are shown in Fig. 12. As before for the One- and Two-Site models, kinetic sorption leads to slower sorption and thus to higher concentrations and earlier solute arrival in the effluent from both regions.

### Discussion

Example calculations for the different types of nonequilibrium were presented. While HYDRUS-1D provides much

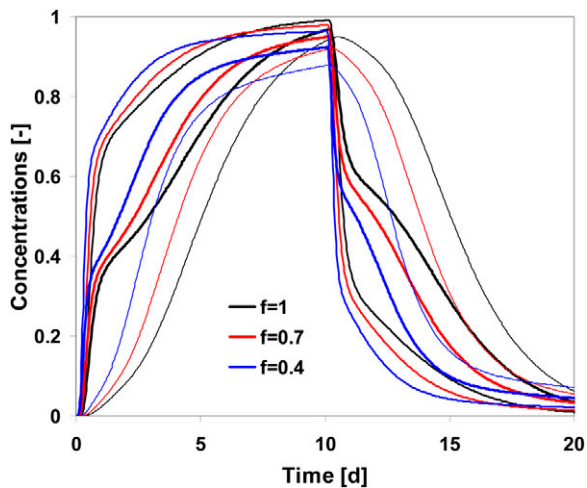


FIG. 12. Breakthrough curves calculated using the Dual-Permeability Model with Two-Site Sorption for a 10-cm-long soil column and the following parameters: solute pulse duration = 10 d,  $q_m = 3 \text{ cm d}^{-1}$ ,  $q_f = 30 \text{ cm d}^{-1}$ ,  $\theta = \theta_m = \theta_f = 0.5$ ,  $w = 0.1$ ,  $\lambda_m = \lambda_f = 1 \text{ cm}$ ,  $K_{dm} = K_{df} = 1 \text{ cm}^3 \text{ g}^{-1}$ ,  $\rho_b = 1.5 \text{ g cm}^{-3}$ ,  $\omega_{dp} = 0.1 \text{ d}^{-1}$ ,  $\alpha_{ch,m} = \alpha_{ch,f} = 0.1 \text{ d}^{-1}$ , and  $f_m = f_f = 1, 0.7,$  and  $0.4$ . Matrix, fracture, and total breakthrough curves are represented by thin, medium, and thick lines, respectively.

information also about the water content and concentration distributions in the soil profile and between different phases (e.g., liquid and solid) and regions (e.g., mobile and immobile, matrix and fracture), here we limited the examples to only calculated breakthrough curves. The calculations, among other things, show that a single breakthrough curve will probably not provide enough information to parameterize models involving both physical and chemical nonequilibrium. Nkedi-Kizza et al. (1984) previously showed that the traditionally used physical and chemical nonequilibrium transport models (i.e., the dual-porosity model with mobile and immobile flow regions and the two-site sorption model, respectively), are mathematically identical when applied to solute breakthrough curves. By analyzing one breakthrough curve, it is hence often not possible to discriminate which process (physical or chemical) is responsible for the observed nonequilibrium process since both types of nonequilibrium can produce the same or very similar results. In that case, one needs additional information, such as breakthrough curves measured simultaneously for a tracer and a reactive chemical, to better analyze the underlying transport processes. Interesting applications of some of these models were presented earlier by Pot et al. (2005) for steady-state water flow conditions and by Köhne et al. (2006) for transient-flow conditions. Both studies were performed on undisturbed soil columns and involved the transport of a nonreactive tracer as well as a reactive pesticide [isoproturon (*N,N*-dimethyl-*N'*[4-(1-methylethyl)phenyl]urea)]. While the tracer breakthrough curves were first used in both studies to characterize the physical conditions of flow process, the pesticide breakthrough curves subsequently provided required information for characterizing the chemical conditions.

Similarly, Bradford et al. (2004) showed that experimental breakthrough curves of colloids or pathogenic microorganisms can be fitted equally well using different models with different assumptions (e.g., attachment vs. straining), and that additional information (in their case, the spatial distribution of colloids) is needed to fully discriminate between the different processes or models. Thorough studies are still needed to evaluate how much and what type of information is required to fully parameterize

selected models. To facilitate such studies, the objective function for the inverse problem in HYDRUS-1D can be formulated in terms of a large number of variables involving not only boundary concentration fluxes, but also water and solute distributions within the soil profile and in different phases (Table 2). For these reasons we believe that HYDRUS-1D is a very attractive tool for analyzing both forward and inverse flow and transport problems.

## Conclusions

We summarized a wide range of nonequilibrium water flow and solute transport models that are available in the latest version of the HYDRUS-1D software package. The models range from classical models simulating uniform water flow and solute transport, to traditional mobile-immobile water physical and two-site chemical nonequilibrium models, to more complex dual-permeability models that consider both physical and chemical causes of nonequilibrium. The presented models form a hierarchical system from which different formulations can be selected for different applications, depending on available information and data.

The various models were divided into three groups: (i) physical nonequilibrium transport models, (ii) chemical nonequilibrium transport models, and (iii) physical and chemical nonequilibrium transport models. Physical nonequilibrium models include the Mobile-Immobile Water Model, Dual-Porosity Model, Dual-Permeability Model, and a Dual-Permeability Model with Immobile Water. Chemical nonequilibrium models include the One Kinetic Site Model, a Two-Site Model, and a Two-Kinetic Sites Model. Finally, physical and chemical nonequilibrium transport models include a Dual-Porosity Model with One Kinetic Site and a Dual-Permeability Model with Two-Site Sorption. The fact that a large number of models has been developed over the years is in many ways reflective of the extremely complicated nature of field-scale processes in which many different physical and chemical processes may combine to lead to nonequilibrium flow and transport.

## Appendix

### Variables for Water Contents and Concentrations

$\theta$	water content [ $L^3 L^{-3}$ ]
$\theta_f$	water content in the macropore (fracture) region of the dual-permeability model (local pore region scale) [ $L^3 L^{-3}$ ]
$\theta_F$	water content in the macropore (fracture) region of the dual-permeability model (global scale) [ $L^3 L^{-3}$ ]
$\theta_{im}$	water content in the immobile region of the dual-porosity and mobile-immobile models [ $L^3 L^{-3}$ ]
$\theta_m$	water content in the matrix region of the dual-permeability model (local pore region scale) [ $L^3 L^{-3}$ ]
$\theta_M$	water content in the matrix region of the dual-permeability model (global scale) [ $L^3 L^{-3}$ ]
$\theta_{m,im}$	water content in the immobile part of the matrix region of the dual-permeability model [ $L^3 L^{-3}$ ]
$\theta_{m,mo}$	water content in the mobile part of the matrix region of the dual-permeability model [ $L^3 L^{-3}$ ]
$\theta_{mo}$	water content in the mobile region of the dual-porosity and mobile-immobile models [ $L^3 L^{-3}$ ]
$c$	liquid-phase concentration [ $M L^{-3}$ ]
$c_f$	liquid-phase concentration in the macropore (fracture) region of the dual-permeability model [ $M L^{-3}$ ]

$c_{im}$	liquid-phase concentration in the immobile region of the dual-porosity model and of the mobile-immobile model [ $M L^{-3}$ ]
$c_m$	liquid-phase concentration in the matrix region of the dual-permeability model [ $M L^{-3}$ ]
$c_{m,im}$	liquid-phase concentration in the immobile part of the matrix region of the dual-permeability model [ $M L^{-3}$ ]
$c_{m,mo}$	liquid-phase concentration in the mobile part of the matrix region of the dual-permeability model [ $M L^{-3}$ ]
$c_{mo}$	liquid-phase concentration in the mobile region of the dual-porosity and mobile-immobile models [ $M L^{-3}$ ]
$S$	solute content in the liquid phase [ $M L^{-3}$ ]
$s^e$	sorbed concentration in equilibrium with the liquid-phase concentration [ $M M^{-1}$ ]
$s^k$	sorbed concentration at kinetic sorption sites [ $M M^{-1}$ ]
$s_1^k$	sorbed concentration at the first fraction of kinetic sorption sites [ $M M^{-1}$ ]
$s_2^k$	sorbed concentration at the second fraction of kinetic sorption sites [ $M M^{-1}$ ]
$s_{im}^e$	sorbed concentration in equilibrium with the liquid-phase concentration in the immobile region of the dual-porosity model [ $M M^{-1}$ ]
$s_{mo}^e$	sorbed concentration in equilibrium with the liquid-phase concentration in the mobile region of the dual-porosity model [ $M M^{-1}$ ]
$s_{mo}^k$	sorbed concentration at kinetic sorption sites in contact with the mobile region of the dual-porosity model [ $M M^{-1}$ ]
$s_m^e$	sorbed concentration in equilibrium with the liquid-phase concentration in the matrix region of the dual-permeability model [ $M M^{-1}$ ]
$s_m^k$	sorbed concentration at kinetic sorption sites in contact with the liquid-phase concentration in the matrix region of the dual-permeability model [ $M M^{-1}$ ]
$s_f^e$	sorbed concentration in equilibrium with the liquid-phase concentration in the macropore (fracture) region of the dual-permeability model [ $M M^{-1}$ ]
$s_f^k$	sorbed concentration at kinetic sorption sites in contact with the liquid-phase concentration in the macropore (fracture) region of the dual-permeability model [ $M M^{-1}$ ]

### ACKNOWLEDGMENTS

This work is based on work supported in part by the Terrestrial Sciences Program of the Army Research Office (Terrestrial Processes and Landscape Dynamics and Terrestrial System Modeling and Model Integration), by the National Science Foundation Biocomplexity Programs no. 04-10055 and NSF DEB 04-21530, and by SAHRA (Sustainability of Semi-Arid Hydrology and Riparian Areas) under the STC Program of the National Science Foundation, Agreement no. EAR-9876800.

### References

- Bradford, S.A., M. Bettehar, J. Šimůnek, and M.Th. van Genuchten. 2004. Straining and attachment of colloids in physically heterogeneous porous media. *Vadose Zone J.* 3:384-394.
- Brooks, R.H., and A.T. Corey. 1964. Hydraulic properties of porous media. *Hydrology Paper 3*. Colorado State Univ., Fort Collins.
- Brusseau, H.L., R.E. Jessup, and P.S.C. Rao. 1989. Modeling the transport of solutes influenced by multiprocess nonequilibrium. *Water Resour. Res.* 25:1971-1988.
- Durner, W. 1994. Hydraulic conductivity estimation for soils with heterogeneous pore structure. *Water Resour. Res.* 30:211-233.
- Gargiulo, G., S.A. Bradford, J. Šimůnek, P. Ustohal, H. Vereecken, and E. Klumpp. 2007. Bacteria transport and deposition under unsaturated

- conditions: The role of the matrix grain size and the bacteria surface protein. *J. Contam. Hydrol.* 92:255–273.
- Gargiulo, G., S.A. Bradford, J. Šimůnek, P. Ustohal, H. Vereecken, and E. Klumpp. 2008. Bacteria transport and deposition under unsaturated conditions: The role of water content and bacteria surface hydrophobicity. *Vadose Zone J.* 7:406–419 (this issue).
- Gerke, H.H., and M.Th. van Genuchten. 1993a. A dual-porosity model for simulating the preferential movement of water and solutes in structured porous media. *Water Resour. Res.* 29:305–319.
- Gerke, H.H., and M.Th. van Genuchten. 1993b. Evaluation of a first-order water transfer term for variably saturated dual-porosity flow models. *Water Resour. Res.* 29:1225–1238.
- Gerke, H.H., and M.Th. van Genuchten. 1996. Macroscopic representation of structural geometry for simulating water and solute movement in dual-porosity media. *Adv. Water Resour.* 19:343–357.
- Hendrickx, J.M.H., and M. Flury. 2001. Uniform and preferential flow mechanisms in the vadose zone. p. 149–187. *In* Conceptual models of flow and transport in the fractured vadose zone. National Academy Press, Washington, DC.
- Jacques, D., and J. Šimůnek. 2005. User manual of the Multicomponent Variably-Saturated Flow and Transport Model HP1. Description, verification, and examples. Version 1.0. BLG-998 Rep. SCK-CEN, Mol, Belgium.
- Jarvis, N.J. 1994. The MACRO model (version 3.1): Technical description and sample simulations. Rep. Diss. 19. Dep. Soil Sci., Swedish Univ. Agric. Sci., Uppsala.
- Köhne, J.M., S. Köhne, and J. Šimůnek. 2006. Multi-process herbicide transport in structured soil columns: Experiment and model analysis. *J. Contam. Hydrol.* 85:1–32.
- Köhne, J.M., B. Mohanty, J. Šimůnek, and H.H. Gerke. 2004. Numerical evaluation of a second-order water transfer term for variably saturated dual-permeability models. *Water Resour. Res.* 40:W07409, doi:10.1029/2004WR003285.
- Kosugi, K. 1996. Lognormal distribution model for unsaturated soil hydraulic properties. *Water Resour. Res.* 32:2697–2703.
- Nkedi-Kizza, P., J.W. Biggar, H.M. Selim, M.Th. van Genuchten, and P.J. Wierenga. 1984. Equivalence of two conceptual models for describing ion exchange during transport through an aggregated Oxisol. *Water Resour. Res.* 20:1123–1130.
- Nkedi-Kizza, P., J.W. Biggar, M.Th. van Genuchten, P.J. Wierenga, H.M. Selim, J.M. Davidson, and D.R. Nielsen. 1983. Modeling tritium and chloride 36 transport through an aggregated Oxisol. *Water Resour. Res.* 19:691–700.
- Pot, V., J. Šimůnek, P. Benoit, Y. Coquet, A. Yra, and M.-J. Martínez-Cordón. 2005. Impact of rainfall intensity on the transport of two herbicides in undisturbed grassed filter strip soil cores. *J. Contam. Hydrol.* 81:63–88.
- Pruess, K. 1991. Tough2: A general-purpose numerical simulator for multiphase fluid and heat flow. Rep. LBL-29400. Lawrence Berkeley Lab., Berkeley, CA.
- Selim, H.M., J.M. Davidson, and R.S. Mansell. 1976. Evaluation of a two-site adsorption-desorption model for describing solute transport in soil. p. 444–448. *In* Proc. Summer Computer Simulation Conf., Washington, DC. 12–14 July 1976. Simulation Councils, La Jolla, CA.
- Selim, H.M., L. Ma, and H. Zhu. 1999. Predicting solute transport in soils: Second-order two-site models. *Soil Sci. Soc. Am. J.* 63:768–777.
- Šimůnek, J., and J.W. Hopmans. 2002. Parameter optimization and nonlinear fitting. p. 139–157. *In* J.H. Dane and G.C. Topp (ed.) Methods of soil analysis. Part 4. Physical methods. SSSA Book Ser. 5. SSSA, Madison, WI.
- Šimůnek, J., D. Jacques, J.W. Hopmans, M. Inoue, M. Flury, and M.Th. van Genuchten. 2002. Solute transport during variably-saturated flow: Inverse methods. p. 1435–1449. *In* J.H. Dane and G.C. Topp (ed.) Methods of soil analysis. Part 4. Physical methods. SSSA Book Ser. 5. SSSA, Madison, WI.
- Šimůnek, J., N.J. Jarvis, M.Th. van Genuchten, and A. Gärdenäs. 2003. Review and comparison of models for describing non-equilibrium and preferential flow and transport in the vadose zone. *J. Hydrol.* 272:14–35.
- Šimůnek, J., M.Th. van Genuchten, and M. Šejna. 2005. The HYDRUS-1D software package for simulating the one-dimensional movement of water, heat, and multiple solutes in variably-saturated media. Version 3.0. HYDRUS Software Ser. 1. Dep. of Environmental Sciences, Univ. of California, Riverside.
- Šimůnek, J., M.Th. van Genuchten, and M. Šejna. 2008. The HYDRUS-1D software package for simulating the one-dimensional movement of water, heat, and multiple solutes in variably-saturated media. Version 4.0. HYDRUS Software Ser. 3. Dep. of Environmental Sciences, Univ. of California, Riverside.
- Šimůnek, J., M.Th. van Genuchten, M. Šejna, N. Toride, and F.J. Leij. 1999. The STANMOD computer software for evaluating solute transport in porous media using analytical solutions of convection–dispersion equation. Versions 1.0 and 2.0. IGWMC-TPS-71. Int. Ground Water Modeling Ctr., Colorado School of Mines, Golden.
- Toride, N., F.J. Leij, and M.Th. van Genuchten. 1993. A comprehensive set of analytical solutions for nonequilibrium solute transport with first-order decay and zero-order production. *Water Resour. Res.* 29:2167–2182.
- van Dam, J.C., J. Huygen, J.G. Wesseling, R.A. Feddes, P. Kabat, P.E.V. van Valsum, P. Groenendijk, and C.A. van Diepen. 1997. Theory of SWAP, version 2.0. Simulation of water flow, solute transport and plant growth in the soil–water–atmosphere–plant environment. Dep. of Water Resour. Rep. 71. Tech. Doc. 45. DLO Winand Staring Centre, Wageningen, the Netherlands.
- van Genuchten, M.Th. 1980. A closed-form equation for predicting the hydraulic conductivity of unsaturated soils. *Soil Sci. Soc. Am. J.* 44:892–898.
- van Genuchten, M.Th. 1981. Non-equilibrium transport parameters from miscible displacement experiments. Res. Rep. 119. U.S. Salinity Lab., Riverside, CA.
- van Genuchten, M.Th., and R.W. Cleary. 1979. Movement of solutes in soils: Computer-simulated and laboratory results. p. 349–386. *In* G.H. Bolt (ed.) Soil chemistry: B. Physico-chemical models. Dev. in Soil Sci. 5B. Elsevier Scientific Publ., Amsterdam.
- van Genuchten, M.Th., and F.N. Dalton. 1986. Models for simulating salt movement in aggregated field soils. *Geoderma* 38:165–183.
- van Genuchten, M.Th., and R.J. Wagenet. 1989. Two-site/two-region models for pesticide transport and degradation: Theoretical development and analytical solutions. *Soil Sci. Soc. Am. J.* 53:1303–1310.
- van Genuchten, M.Th., and P.J. Wierenga. 1976. Mass transfer studies in sorbing porous media: I. Analytical solutions. *Soil Sci. Soc. Am. J.* 40:473–481.